STRUCTURAL AND BIOCHEMICAL INSIGHTS INTO THE INHIBITION OF HUMAN ACETYLCHOLINESTERASE BY G-SERIES NERVE AGENTS AND SUBSEQUENT REACTIVATION BY HI-6

by

JACK MCGUIRE

(Under the Direction of Scott Pegan)

ABSTRACT

The toxicity of irreversible human acetylcholinesterase inhibition, via G-series nerve agents, potentially relies on the unique accommodation of the inhibitor. Therapeutic compounds that reverse human acetylcholinesterase (hAChE) inhibition, known as reactivators, vary in efficacy depending on multiple factors including the particular nerve agent present. The oxime reactivator, HI-6, shows particularly low activity on tabun (GA)-inhibited hAChE, but can reactivate hAChE inhibited by other G-series agents to varying degrees, including sarin (GB) and soman (GD). To gain insight into this issue, the structures of hAChE inhibited by tabun, sarin, cyclosarin, soman, and GP were obtained though X-ray crystal diffraction. In addition, the inhibition and reactivation kinetics for these agents were obtained through the use of a modified Ellman's assay. To identify the structural underpinnings of this phenomenon, the structures of tabun, sarin, and soman-inhibited hAChE in complex with HI-6 were determined. This revealed the impact of the nerve agent adduct on reactivator access and placement within the active site. These insights will contribute towards a path of next generation reactivators and an improved understanding of the innate issues with the current reactivators.

INDEX WORDS: Acetylcholinesterase, G-series, Nerve Agent, HI-6, Reactivator, tabun, soman, sarin, cyclosarin, GP,

STRUCTURAL AND BIOCHEMICAL INSIGHTS INTO THE INHIBITION OF HUMAN ACETYLCHOLINESTERASE BY G-SERIES NERVE AGENTS AND SUBSEQUENT REACTIVATION BY HI-6

by

JACK MCGUIRE

B.S., The University of Georgia, 2020

A Thesis Submitted to the Graduate Faculty of The University of Georgia in Partial Fulfillment of the Requirements for the Degree

MASTER OF SCIENCE

ATHENS, GEORGIA

2020

STRUCTURAL AND BIOCHEMICAL INSIGHTS INTO THE INHIBITION OF HUMAN ACETYLCHOLINESTERASE BY G-SERIES NERVE AGENTS AND SUBSEQUENT REACTIVATION BY HI-6

by

JACK MCGUIRE

Major Professor:	Scott Pegan
Committee:	William Lanzilotta
	Brian Cummings

Electronic Version Approved:

Ron Walcott
Interim Dean of the Graduate School
The University of Georgia
May 2020

ACKNOWLEDGEMENTS

I would like to take the time to acknowledge all of the help and support that has brought me this far. My family has been one of my biggest supporters, allowing me to pursue my dreams and providing me with the resources needed to do so. Additionally, my current and past lab members have aided me in too many ways to count. I owe a large amount of my success and knowledge to Stephanie Bester and Dr. Scott Pegan. Each of them worked tirelessly and diligently to ensure I was able to conquer every problem I faced. They did not give up at any time, no matter how hard I struggled. I wish to acknowledge them and show them how much I appreciate their help throughout the years.

TABLE OF CONTENTS

Page

APPENDICES

LIST OF TABLES

Page

LIST OF FIGURES

Page

CHAPTER 1

INTRODUCTION

Throughout history there have been numerous creations, whether they be accidental or purposefully, within the realm of Weapons of Mass Destruction (WMD). WMD's are defined as weapons that can kill and bring significant harm to many humans and/or cause a large amount of damage to man-made structures, natural structures, or the environment at large[1]. Under the classification of a WMD, is chemical warfare. Chemical warfare has been noted as one of the most vicious Weapons of Mass Destruction created by mankind. These agents have either lethal or incapacitating effects on humans and are caused via shear force and usually localized[2].While utilizing poisons from plants to poison individuals has been recorded and documented during the 14^{th}, 15^{th}, and 16^{th} centuries, the widespread use of chemical warfare did not fully develop until the 19^{th} century. During this period of time, Germany used chlorine gas to attack Ypres, Belgium in 1915. Throughout World War I, chemical warfare (including phosgene and sulfur mustard) caused approximately 100,000 deaths and over one million causalities.[3] It was not until the 1930's when a German chemist, Gerhard Schrader, was studying organophosphate insecticides and discovered the first known nerve agent, tabun.

Nerve agents today

Nerve agents are very deadly chemical compounds known to quickly cause paralysis and death. Today there is still a threat to our military personnel as well as to the public. In 2017, Kim Jong-Nam was assassinated with the nerve agent commonly known

as VX[4]. Even more recently, a former Russian military intelligence officer and his daughter were poisoned with nerve agents on March 4, 2018 in Salisbury, UK[5]. Furthermore, the war Syria has proved to be extremely fatal with the continued use of nerve agents. Over 30 total attacks have been confirmed by the UN Commission of Inquiry as of April 2018[6].

In 1936, the first nerve agent commonly known as Tabun (GA), was synthesized. Since then a multitude of different nerve agents and nerve agent classes have been created. The two well-known classes of these are categorized under the G-series nerve agents and the V-series nerve agents. G-series nerve agents were synthesized in Germany during World War II from the 1930's to the 1940's. These include tabun, sarin (GB), soman (GD), cyclosarin (GF), and GP. The V-series agents were created in the United Kingdom during the 1950's, including VX, VE, VG, VM, VP, VR, VS and others. There is, however, a third class of nerve agents publicly known as Novichok agents[5, 7].

Mechanism of action

While there are a multitude of nerve agents, they all act upon the human body in a similar way. The primary cholinesterase in the body is known as the enzyme acetylcholinesterase (AChE). In a healthy body, the neurotransmitter acetylcholine (ACh) targets nicotinic and muscarinic receptors found in the postsynaptic neuron. Once acetylcholine binds to these receptors and activates them, acetylcholinesterase breaks down ACh into acetate and choline in order to end activation. Choline is then transported back into the presynaptic neuron where it is used to be synthesized into ACh again. When one is exposed to nerve agents, the nerve agents bind to AChE and heavily inhibits it. Once AChE is inhibited, it is unable to breakdown ACh. Without the breakdown of ACh,

the nicotinic and muscarinic receptors are continuously being activated. Unfortunately, with the constant activation of these receptors, a cascade of debilitating symptoms begins to erupt. One experiences headaches, muscle spasms, vomiting, seizures, coma, and if not treated quickly death is likely.

All nerve agents act in a similar way due to the shared chemical composition between them. Nerve agents share an organophosphate core which allows them to effectively inhibit acetylcholinesterase. Due to this, nerve agents are able to covalently bond to one of the active sites within AChE and hinder its functions. AChE contains a catalytic triad made up of a serine, histidine, and glutamate where ACh is able to bind and be further broken down. Nerve agents take advantage of the serine hydrolase within this triad. Additionally, this active site contains three significant areas known as the oxyanion hole, the anionic site, and the acyl binding pocket (Figure 1.1). All three of these effectively accommodate the present molecule, whether it be ACh or a nerve agent, and provide potential intermolecular interactions to further stabilize the nerve agent or aid in the breakdown of ACh.

When a nerve agent enters the active site, they first phosphorylate AChE and bind to the serine. Once inhibited, there are two pathways AChE can take (Figure 2.8). If treatment is administered quickly (and is effective), AChE can be reactivated and a phosphyloxime will be broken off of AChE and its function will be restored. If no treatment is administered, AChE will go through dealkylation and become aged. At this point, current reactivators are unable to revert the inhibition. However, new studies into resurrection agents have shed some light and hope into reversing the aged state[8, 9].

The reactivator dilemma

Current reactivators have limited effectiveness due to the varying nerve agent possibilities. Each nerve agent impacts AChE in different ways, suggesting conformational and electrostatic changes within the active site. This is why it is difficult to create a reactivator effective in reactivating a multitude of different agents. Additionally, reactivators pose other threats such as toxic intermediates, potentially dangerous inhibition of native AChE, and the inability to reactive aged AChE. There is a significant degree of variation in the current reactivator's therapeutic efficacy. The actual reactivator used with the United State's military is known as obidoxime (2-PAM). The cocktail of pralidoxime (2-PAM) and atropine is reasonably effective against some nerve agents, however not highly effective at any of them. HLö-7 demonstrates greater reactivation, but until recently it had been difficult to produce. HI-6 is used with the Canadian military, but demonstrates similar effectiveness to 2-PAM[10]. Due to the lack of effective reactivation across all nerve agents, the need for a new and optimized reactivator is required.

Researching AChE

In order to accurately analyze AChE and its kinetic abilities, Ellman's assays were employed. The Ellman's assay is an indirect method of measuring acetylcholinesterase. It is a standard colorimetric assay which can be modified to use an inhibitor or a reactivator (Figure 1.2). Once performed, a quantifiable yellow colored product is produced (TNB^2). Acetylthiocholine (ACTh) acts similarly to acetylcholine, which is broken down by AChE to form choline and acetate. In this assay ACTh is used instead of ACh because it forms TNB^2 or 2-nitro-5-thiobenzoate via its hydrolysis, which

is able to be measured as the increase in the absorbance of TNB^2. Utilizing a spectrophotometer or plate reader at 412 nm, the absorbance is able to be measured and further calculations can be performed. For example, in a 96 or 384 well plate, a 50mM phosphate buffer with BSA (1mg/ml) is used to house AChE. Next an addition of DTNB into the well. When ready to start the reaction, add ATCh and quickly place it in the plate reader or spectrophotometer. What happens is the creation of TNB2- via the hydrolysis of acetylthiocholine (ATCh). This is able to be measured as the increase in absorbance of TNB^{2-} at 412 nm. Throughout AChE research, Ellman's assays are generally the accepted method of assessing ache activity. This assay is used by numerous researchers throughout the studying of acetylcholinesterase and is widely respected to accurately display its kinetic abilities.

To further analyze the data obtained from Ellman's assays, a slew of calculations was employed. The exact details of how the reactions were specifically laid out and the specifics within the wells of the assay plate are described in Chapter 2: Materials and Methods. Naturally, once the assays were performed and the raw data was obtained, calculating the percent reactivated AChE can begin. The change in percent reactivated AChE is proportional to the rate of hydrolysis of acetylthiocholine relative to uninhibited AChE. The rate of reactivation (k_{obvs}) at each concentration is given by Figure 1.3 which assumes complete inhibition. All experiments were performed in triplicate. After that, the percent reactivated was determined according to Figure 1.4, where v_t is the rate of reaction of thiocholine with DTNB at time t, v_{ox} is the rate of reaction of oxime with DNTB at each concentration measured, and v_o is the rate of reaction of thiocholine with DTNB at time t for uninhibited AChE. The rate of reaction of thiocholine with DTNB

was taken as the rate of the hydrolysis of acetylthiocholine to thiocholine and acetate. Additionally, Figure 1.5 is used where k_{obvs} is the first-order reactivation rate constant, t is the time at which the assay solution was added to the reactivated AChE, and A is the theoretical percent of maximum reactivation. Lastly Figure 1.6 and 1.7 demonstrate where K_{ox} and k_2 were determined from the second-order plot of k_{obvs} and oxime concentration, where k_2 is the intrinsic reaction constant; K_{ox} is the apparent equilibrium constant, and k_r is the second-order reactivation rate constant[11]. Following these equations, we are able to obtain the kinetic abilities of human acetylcholinesterase.

The first structural information of acetylcholinesterase originate from the crystallization of AChE from the pacific ray eel, *torpedo* californica[12]. Since then several other species of AChE have been purified and studied such as mouse, pig and guinea pig. Eventually, the ability to purify human acetylcholinesterase was perfected and research exploded from there. It was noted that the active site of AChE is highly conserved among the species and were used as models before. Surprisingly, the activity and accommodation of adducts were incomparable. Therefore, these models were not particularly accurate when used to predict human AChE activity. Understanding that each nerve agent varies in it reactivation and active site accommodation, using any other model besides human AChE would be meaningless.

In order to further understand nerve agents and their ability or inability to be reactivated, meticulous research with hAChE needed to be performed. The class of nerve agents known as the G-series provided a perfect example of this variability. It has been demonstrated that tabun is extremely difficult to reactivate with the current treatments while a similar nerve agent, sarin, is readily reactivated. Additionally, there were three

other agents within the G-series class with very little research behind them. This provided an opportunity to gain knowledge behind the molecular underpinnings of these nerve agents and understand the reasoning behind their variability.

Figures

Figure 1.1 AChE active site

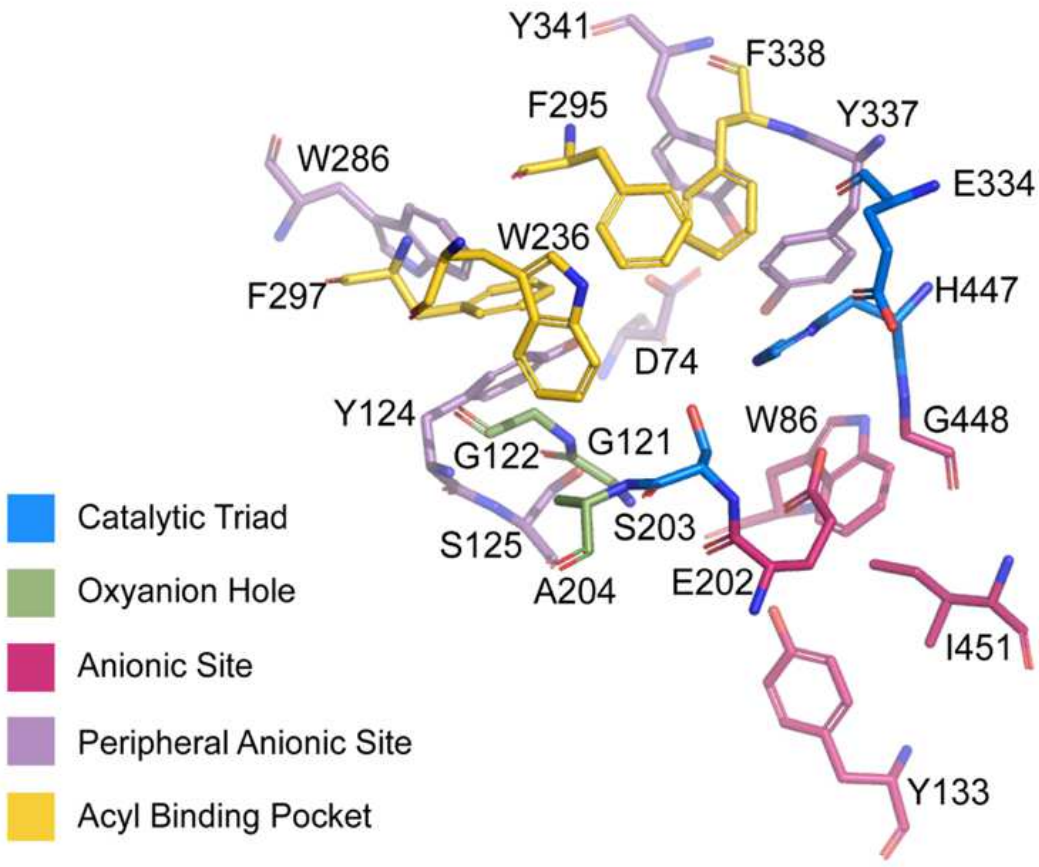

Figure 1.2 Ellman's Assay

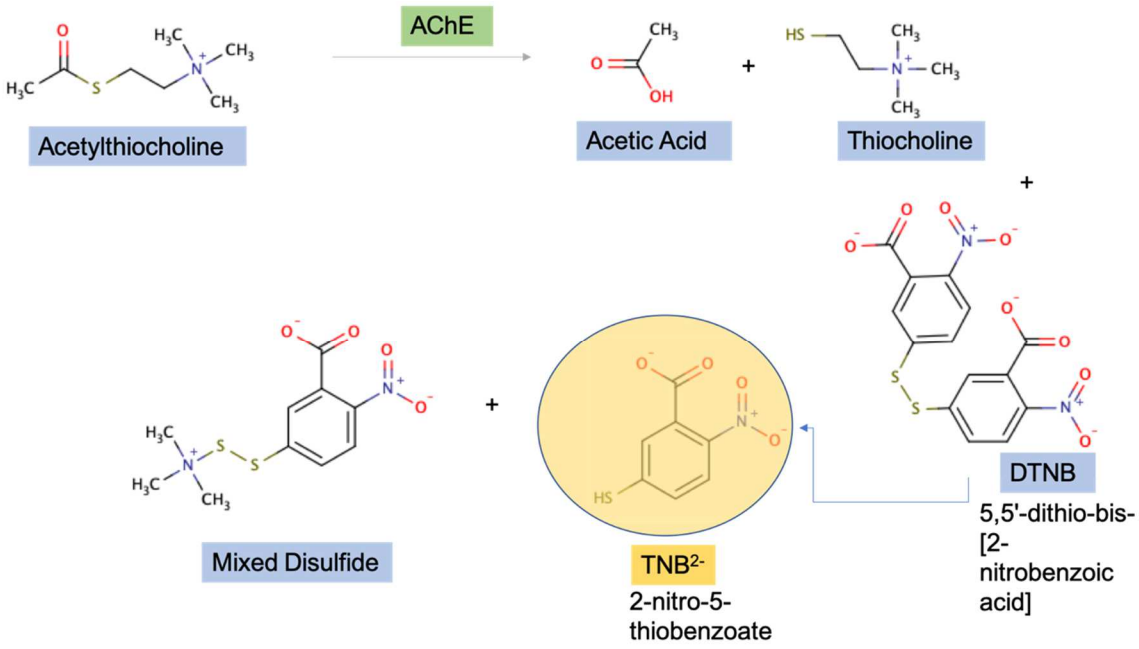

Figure 1.3 Equation 1

$$-k_{obvs}t = \ln\left(\frac{v_o - v_t}{v_o - v_{ox}}\right)$$

Figure 1.4 Equation 2

$$(E_{react})_t = \frac{v_t - v_{ox}}{v_o - v_{ox}}$$

Figure 1.5 Equation 3

$$E_{react}t = A(1 - e^{-k_{obvs}t})$$

Figure 1.6 Equation 4

$$k_{obvs} = \frac{k_2}{1 + K_{ox}/[ox]}$$

Figure 1.7 Equation 5

$$k_r = \frac{k_2}{K_{ox}}$$

CHAPTER 2

STRUCTURAL AND BIOCHEMICAL INSIGHTS INTO THE INHIBITION OF HUMAN ACETYLCHOLINESTERASE BY G-SERIES NERVE AGENTS AND SUBSEQUENT REACTIVATION BY HI-6*

To be submitted to Chemical Research in Toxicology

Jack R. McGuire[1], Stephanie M. Bester[1], Mark A. Guelta[2], Jude Chenge[1], Mark Winemueller[2], Sue Bae[2], James Myslinski[2], Scott D. Pegan[1], and Jude J. Height*[2]

[1]Department of Pharmaceutical and Biomedical Sciences, University of Georgia, Athens, Georgia 30602, UGA. [2]U.S. Army Edgewood Chemical Biological Center, Aberdeen Proving Ground, MD 21010-5424, USA.

Abstract

The recent use of organophosphate nerve agents in Syria[6], Malaysia[4], and the United Kingdom[5] has reinforced the potential threat of their intentional release. These agents act through their ability to inhibit human acetylcholinesterase (hAChE; E.C. 3.1.1.7), an enzyme vital for survival. The toxicity of irreversible human acetylcholinesterase inhibition, via G-series nerve agents, potentially relies on the unique accommodation of the inhibitor. Utilizing racemic mixtures of inhibitors, the nerve agent generally adopts a conformation very similar to its most toxic conformation within the active site, demonstrated by Bester[13]. Therapeutic compounds that reverse hAChE inhibition, known as reactivators, vary in efficacy depending on multiple factors including the particular nerve agent present. The oxime reactivator, HI-6, shows particularly low activity on tabun (GA)-inhibited hAChE[14], but can reactivate hAChE inhibited by other G-series agents, including sarin (GB) and soman (GD). To gain insight into this issue, the structures of hAChE inhibited by tabun, sarin, cyclosarin, soman, and GP were obtained though X-ray crystal diffraction. In addition, the inhibition kinetics for these agents were obtained through the use of a modified Ellman's assay. Through this information, the role of hAChE active site plasticity in agent selectivity is revealed. With reports indicating that the efficacy of reactivators can vary based on which nerve agent inhibits hAChE[15], the use of modified Ellman's assays highlighted these efficacy variations among tabun, sarin, and soman. To identify the structural underpinnings of this phenomenon, the structures of tabun, sarin, and soman-inhibited hAChE in complex with HI-6 were determined. This revealed the impact of the nerve agent adduct on reactivator access and placement within the active site to include unproductive poses of HI-6. These insights will contribute towards

a path of next generation reactivators and an improved understanding of the innate issues with the current reactivators.

KEYWORDS: Acetylcholinesterase, G-series, Nerve Agent, HI-6, Reactivator, tabun, soman, sarin, cyclosarin, GP

Introduction

Nerve agents pose a persistent threat to humans through the threat of their intentional release[16]. The recent events in Syria[6] and Malaysia[4] underscore this potential threat. Additionally, this impending threat was, again, reaffirmed by the nerve agent attack against the Russian defector Skripal in Salisbury, England[5].

Acetylcholinesterase is a vital enzyme that catalyzes the hydrolysis of the neurotransmitter acetylcholine (ACh) to control the level of ACh and nerve signaling. This enzyme locates itself within the neuromuscular junction (NMJ) of all autonomic ganglia and innervated organs, the brain and spinal cholinergic synapses [8]. Due to its essential role in the nervous system, inhibiting AChE has been a popular target for pesticide and chemical warfare development [9]. Currently developed nerve agents and pesticides rely on the same organophosphate core to covalently modify acetylcholinesterase's catalytic serine leading to inhibition and in most cases can result in additional processes that age the enzyme. For example, G-type nerve agents such as soman (*O*-pinacolyl methylphosphonofluoridate) possess the same fluorophosphate moiety as the pesticide mipafox (N,N'-Diisopropyldiamidofluorophosphate; DDFP). Numerous other nerve agents belong to the same class as soman (GD), such as tabun, sarin, cyclosarin and GP. Each of these possess the same fluorophosphate moiety with differing side groups uniquely characterizing their

inhibitory properties and their ability to be reactivated. Inhibition of AChE includes two steps, an initial inhibition, then eventual aging of the AChE enzyme (Figure 2.8). Potential reactivation of AChE from its inhibited state is possible through the use of an oxime-based reactivator such as, 2-PAM, which has been a popular therapeutic route.

Interestingly, there are very few published structures entailing the non-aged form of these G-series nerve agents inhibiting human acetylcholinesterase. Naturally, structures of G-series inhibited hAChE of other species including Pacific electric ray and mouse exist. The toxicity of these nerve agents have been demonstrated to vary from species to species[17], which made direct comparisons to hAChE difficult. Previous research demonstrated GA-inhibited hAChE to exhibit extreme resistance to reactivation via the oxime reactivator HI-6[14]. It has been speculated that GA might impact hAChE's active site differently than other G-series agents as most reactivators have limited effectiveness towards it[18]. Unlike GA, GB-inhibited hAChE appears to readily reactivated in the presence of HI-6 as the reactivator, while GF-inhibited hAChE is even more prone to reactivation via HI-6[10]. Intriguingly, GD-inhibited hAChE has proven very difficult to reactivate via numerous reactivators including HI-6[19]. Previous research discovered that the G-series nerve agent soman exhibits a spontaneous and extremely rapid dealkylation reaction or aging process which, in turn, blocks reactivation via oximes. With each G-series agent exhibiting its own unique inhibitory and reactivation characteristics, it is crucial to obtain a better structural and kinetic understanding of them.

This study aims to provide insight into the sources of variations involved in the ability to reactivate between each G-series nerve agents. As a result of this, multiple G-series agent's (GA, GB, GD, GF, GP) ability to inhibit isolated hAChE expressed in HEK-

293 cells were assessed. Furthermore, the efficiency of HI-6 to reactivate inhibited hAChE was also explored. Employing x-ray crystallography, six structures of inhibited hAChE were obtained with conjugates of GA, GB, GD, GF, and GP. Additionally, three structures of inhibited hAChE with conjugates of GA, GB, and GD in complex with HI-6 (hAChE-GA-HI6) were obtained. Through these developed structures and with the help of enzymatic kinetic data, critical insights into the molecular underpinnings of each G-series nerve agent's impact on the active site were analyzed and the influence it had on reactivatability.

Results

G-series Inhibition of hAChE

The k_{cat} for AChEs processing acetylcholine is known to have an extraordinarily broad range from as low as 12000/s to over 500,000. Beyond differences between species, multiple variables have been observed to dramatically change the turnover rate of AChE for its substrate; this includes pH, ionic strength, and lastly method of purification. This has proven particularly problematic for evaluating hAChE's underlying catalytic efficiency as well as nerve agent's potency towards the enzyme. With the inability until recently to obtain pure recombinant human expressed hAChE, previous studies relied on the use of erythrocyte ghosts. Although this system has provided considerable insight into relative potency of agents, the concentration of active hAChE within these ghosts is often difficult to standardize. Additionally, there are needs to address butylcholinesterase activity and other confounding factors that can vary in this type of system[15, 20]. To side step these issues and obtain a more direct measure of the kinetics involved in hAChE inhibition by

nerve agents, purified recombinant hAChE was expressed and purified from HEK-293 cells.

Utilizing a modified Ellman's assay, hAChE's k_{cat} towards acetylcholine was determined to be 104,636 s^{-1}. With the uninhibited activity established for hAChE, similar assays were employed to determine potency of the racemic mixtures of GA, GB, GD, GF, and GP. These assay's yielded a k_i of 2.3 x 10^6 M^{-1} min^{-1}, 1.1 x 10^7 M^{-1} min^{-1}, 4.4 x 10^7 M^{-1} min^{-1}, 4.6 x 10^8 M^{-1} min^{-1}, and 8.9 x 10^6 M^{-1} min^{-1} respectively (Table 2.1). While the k_i of each are mostly similar, tabun has the lowest of the G-series agents which might provide some insight as to why GA is so difficult to reactivate. Additionally, GB is readily reactivated via HI-6, GD demonstrates moderate levels of reactivation, while GA produces only a mere seven percent reactivation which leads to the need for structural insights for distinctions.

Structural insights of G-series inhibited hAChE

Knowing that each G-series nerve agent produces unqiue biochemical characteristics, the molecular underpinnings of these features were investigated. Consequently, hAChE dimer was crystallized and then soaked in a solution containing 6.17 mM of a racemix mixture of tabun was soaked for 7 minutes prior to freezing. These crystals led to obtaining a 2.63 Å dataset in space group $P3_121$ that was subsequently solved using apo hAChE (PDB 4EY4)[21] as a search model (Table 2.2). Similar to other hAChE crystal structures, two monomers were found in the asymmetric unit. Upon examination of the active sites, significant F_o - F_c simulated annealing omit map density was observed at the OG atom of Ser203 in both active sites (Figure 2.3a). The initial density near Ser203

housed the tabun adduct considerably well, and throughout refinement the density only improved.

The GA adduct appears to adopt an orientation that is similar to most organophosphate compounds.[13, 22, 23] Detailing tabun's interactions, its ethoxy group points towards the large hydrophobic pocket consisting of Tyr133, Trp86, Tyr337, and Phe338, whereas the disubstituted nitrogenous group points to the relatively smaller hydrophobic pocket of Phe295, W236, and F297. Within hAChE's oxyanion hole, tabun's carbonyl oxygen forms hydrogen bonds with Gly122, Gly121, and Ala204. Further investigation denotes a hydrogen bond formed between the ethoxy oxygen of tabun and His447 of hAChE. Interestingly, these interactions form what appears to be the catalytic triad expected to form between the natural substrate of hAChE, acetylcholine (ACh), and hAChE.

To further understand how structural differences, influence the unique biochemical characteristics the G-series nerve agents produce, hAChE dimer was crystallized and further soaked in a solution containing 42.83 mM GB for 1 minute. These crystals led to a 2.46 Å dataset in space group $P3_121$ that was also solved utilizing hAChE (PDB 4EY4)[21] as a search model (Table 2.2). In detail, sarin appears to form hydrogen bond interactions with its carbonyl oxygen and Gly122, Gly121, and Ala204 throughout the oxyanion hole (Figure 2.3a). Moreover, GB's methyl group is oriented toward the small hydrophobic pockets, while its isopropyl group points itself towards the a large hydrophobic pocket. Sarin appears to make similar intermolecular interactions with hAChE relative to what tabun demonstrated.

Furthermore, additional hAChE dimer was crystallized and further soaked in a solution containing 10mM GD for 1 minute. These crystals led to a 2.55 Å data set in space group $P3_121$ solved with the same hAChE model (PDB 4EY4)[21] as a search model (Table 2.2). Just as GA and GB exhibited, GD's carbonyl oxygen forms hydrogen bond interactions with the oxyanion hole of Gly122, Gly121, and Ala204 (Figure 2.3c). Additionally, GD's methyl group is pointed towards the small hydrophobic pocket of Phe295, W236, and F297, while its bulky carbonous group is positioned towards the large hydrophobic pocket of Y337, W86, Y133, and F338. To gain additional insight into how hAChE accommodates other G-series nerve agents, cyclosarin (GF) and 2,2′-dimethylcydopentyl methylphosphonofluoridate (GP) inhibited hAChE were crystallized. Crystallized hAChE dimer was soaked with 33.3 mM GF for 30 minutes while additional hAChE dimer was soaked with 10mM GP for 2 minutes. These crystals led to a 2.31 Å and a 2.30 Å dataset, respectively, in space group $P3_121$ solved with that same hAChE model (PDB 4EY4)[21] as a search model (Table 2.2). Once again, we observe similar interactions within the active site. Both GF and GP form hydrogen bond interactions with His447 and throughout the oxyanion site including Gly122, Gly121, and Ala204 (Figure 2.3d and 2.3e). Similar to GB and GD, both GF and GP position their larger carbonous side group toward the large hydrophobic pocket in the active site, while their methyl group is oriented toward the smaller hydrophobic pocket. Overall, it appears that these G-series nerve agents demonstrate similar structural interactions with hAChE's active site which does not explicitly propose an answer for the varying ability to reactivate between the agents and the enzymatic data.

Although superficially it appears that these structures are mostly equivalent, there are some differences that potentially impact hAChE. When overlaid (Figure 2.4a) the accommodation of GA's larger nitrogenous side group into the small hydrophobic group likely produces this noticeable shift of Phe295. Previously it has been demonstrated, with VX (P_R), that a shift in Phe295 similar to this can influence the k_i.[13] Even though the shift in Phe295 is only approximately 1.0 Å (Figure 2.5), it causes a minor shift of residues Arg296 and F297 which was also seen with VX (P_R). Another significant difference is the hydrogen bond length between the side group's, oriented towards the large hydrophobic pocket, oxygen with His447. Within GB and GD-inhibited hAChE, the bond length is greater than 3.0 Å, however tabun creates a significantly shorter bond of 2.5 Å. Furthermore, there is a large shift in the orientation of GF-inhibited hAChE's Phe338 relative to the other G-series nerve agent's hAChE. These structural differences further support the lower k_i exhibited by GA-inhibited hAChE. With this information allowing us more detailed information on the inner workings of G-series nerve agents, a greater understanding of their ability to reactivate could be drawn from structures in complex with such reactivators.

HI-6 Bound to the Active Site of G-series-inhibited with hAChE

Such structures were created by crystallizing dimer hAChE and soaking the crystal in 24.67 mM GA for 1 minute and an 11.1 mM HI-6 solution for 1 minute. These crystals led to a 2.46 Å dataset in space group $P3_121$ that was also solved utilizing hAChE (PDB 4EY4)[21]. Within GA-inhibited hAChE in complex with HI-6, two conformations of HI-6 were present. The major differences between these two lie in the peripheral anionic site (PAS) of hAChE. The PAS is near the tail-end pyridinium ring of HI-6 including residues

such as Trp286, Tyr72, and Tyr124. The first HI-6 conformation found in GA had its tail-end pyridinium ring between both Trp286 and Tyr72 producing stacking interactions. The other conformation of HI-6 produces stacking with Trp286 and Tyr124. Both of these orientations within the PAS site are facilitated by the significant conformational rearrangement of Trp286 that creates a 3.0 Å wide gap of the PAS that allows HI-6 to access the active site.[13] These different conformations also allow for varying hydrogen bond interactions with the tail end nitrogen and carbonyl oxygen, where the first conformation interacts with Glu385, while the second interacts with Trp286 and Ser298. Further into hAChE's active site HI-6's oxime arm makes other hydrogen bond interactions with Tyr124, and a water allowing it to stabilize itself within this orientation. Additionally, the pyridinium ring further into the active site appears to form stacking interactions with Tyr341, furthering its stabilization. One of these conformations is very similar to a productive HI-6 conformation found when bound to $P_{R/S}$-VX-inhibited hAChE known as HI-$6_{1[13]}$. Although HI-6's second conformation within GA-inhibited hAChE differs inside the PAS, its effect on the pyridinium ring further in the active site is minute, demonstrated by its distance into the active site being relatively equal.

To further distinguish G-series inhibited hAChE's ability to reactivate, the apo crystal was soaked in a buffer with 28.55 mM GB for 2 minutes and then a buffer with 11.1 mM HI-6 for 2 minutes. These crystals led to a 2.37 Å data set in space group $P3_121$ that was solved utilizing hAChE (PDB 4EY4)[21]. Inside GB-inhibited hAChE's in complex with HI-6 we see two conformations of HI-6 that are similar to those within GA-inhibited hAChE in complex with HI-6. The first conformation involves Tyr72 and Trp286 in its PAS along with hydrogen bond interactions with Glu285 and its tail-end pyridinum

ring in order to provide stabilization in the active site. The second conformation of HI-6 includes Tyr124 and Trp286 instead of Tyr72, within its PAS, due to the conformational rearrangement ability of Trp286 to accommodate orientations such as this. The tail-end pyridinium ring of the second conformation also makes hydrogen bond interactions with Glu285, while also interacting with Ser298 and a nearby water to further its stabilization. Moving further into the active site, the first conformation of HI-6 forms hydrogen bond interactions with its pyrdinium ring's nitrogen and Tyr124. Naturally, the second conformation of HI-6 loses this interaction due to its PAS arrangement and instead, forms hydrogen bond interactions with Tyr124 and its linker oxygen. Both of the conformations of HI-6 form similar interactions with their oxime arm and Phe295, as well as potential stacking between their second pyridinium ring and Tyr341 providing significant stabilization deeper into the active site. Interestingly, the first conformation of HI-6 within GB-inhibited hAChE exhibits a similar spatial arrangement as HI-6_3 demonstrates when bound to $P_{R/S}$-VX-inhibited hAChE.

The final G-series nerve agent crystallized to investigate inhibited hAChE's reactivation via HI-6 was GD. The apo crystal was soaked in a buffer with 24.67 mM GD for 2 minutes and then a buffer with 11.1 mM HI-6 for 2 minutes. These crystals led to a 2.20 Å data set in space group $P3_121$ that was solved utilizing hAChE (PDB 4EY4)[21]. Intriguingly, there was only one conformation of HI-6 within GD-inhibited hAChE. This conformation of HI-6 produced PAS stacking interactions involving Tyr72 and Trp286 as well as potential hydrogen bond formations with HI-6's tail-end, Val282, and a nearby water. Further into the active site similar interactions with the second pyridinium ring are formed. The nitrogen of this pyridnium ring forms hydrogen bonds with Tyr124. The

nitrogen within this pyridinium ring's oxime arm also forms hydrogen bonds with Tyr 124, while the oxygen of this arm forms hydrogen bond with a nearby water. Additionally, there is potential between this second pyridinium ring and Tyr341. Remarkably, the conformation of HI-6 found within GD-inhibited hAChE also is similar to the HI-6_1 exhibited when HI-6 is in complex with $P_{R/S}$-VX-inhibited hAChE. To advance our investigation of the structural differences between G-series nerve agent's inhibition and their effect on potential reactivation, more detailed structural analysis was required.

In order to understand the molecular underpinnings of each G-series nerve agent and their particular effects on hAChE and reactivation, minor changes needed to be considered. At first blush, it appears that each HI-6 is generally occupying the same area. Naturally, there are subtle differences between them, most importantly how HI-6_{GB} is further into the active site relative to HI_{GA} and HI-6_{GD}. Within both conformations, HI-6_{GB} is allowed to dive deeper into the active site which further supports its higher percent reactivation found in the enzymatic data. Additionally, Tyr341 exhibits stacking between itself and the second pyridinium ring of HI-6. Within both conformations of GA/GB-inhibited hAChE the Tyr341 of GA/GD-inhibited hAChE are further downward, relative to GB-inhibited hAChE's Tyr341. Another interesting variance between the three G-series-inhibited hAChE's is residue Tyr337. In both conformations of GA and GB, the Tyr337 of GA-inhibited hAChE is further downward relative to GB. Similarly, the Tyr337 within GD-inhibited hAChE is further downward as well as leftward relative to GB. Other small differences lie within residue Tyr124. GB-inhibited hAChE's Tyr124 is further toward Ser203 while both GA and GD-inhibited hAChE's Tyr124 is further leftward, most likely due to the relative distance to the second pyrindinium ring due to the possible t-shaped

stacking. Interestingly, a similar Phe295 shift is demonstrated in GA-inhibited hAChE in complex with HI-6 as seen in only GA-inhibited hAChE. Acknowledging all of these variations between each G-series nerve agent-inhibited hAChE allows us to further understand the molecular foundations of each structure while gaining knowledge on their effects on the ability for reactivation.

Discussion

Structural Impact of G-series Nerve Agents

With the little structural information on G-series nerve agents throughout the field, these structures can provide us with a foundation of knowledge to better understand the G-series agents. Previous research has indicated that there is heavy difficulty when reactivating GA with HI-6, however GB is readily reactivated and additionally denotes that GD is prone to extremely rapid aging.[18] When analyzing the variations between only GA/GB/GD-inhibited hAChE, there are not too many noticeable differences except for the shift in Phe295. Both GD and GB's larger side group is oriented toward the larger hydrophobic pocket of Tyr133, Trp86, Tyr337, and Phe3388, whereas GA's larger (and nitrogenous) side group is angled toward the small hydrophobic pocket of Phe295, Trp236, and Phe297. Due to this large charged group pointed toward the smaller hydrophobic pocket, it appears to force Phe295 away from the inhibitor. This shift outward from the active site is similar to the more toxic enantiomer of VX known as P_R-VX.[13] It has been demonstrated that the structural disturbance of certain active site residues including Phe295 and Arg296 may block an oxime's access to the inhibitor resulting in inefficient reactivation[24]. Another noticeable difference between the active sites is GF-inhibited

hAChE's shift of Phe338. It appears that because of GF's orientation of its side groups, Phe338 is allowed an opening within the active site. While observing the other G-series nerve agents, either the side group oriented toward the small hydrophobic pocket is hindering Phe338's movement or the side group oriented towards the large hydrophobic group is positioned far enough away from Phe338, unlike GF. It seems that GF-inhibited hAChE presents the perfect opportunity for Phe338 to further itself within the active site. With this major conformational change, it appears that Phe338 essentially aids to lock GF within the active site which could cause the noticeable elevation of its k_i. Throughout each G-series-inhibited hAChE, there were not a multitude of differences. Naturally, the few spatial arrangement variations present, appear to explain the lows and highs of the k_i's while also developing a better understanding of how each nerve agent affects hAChE in its own method.

Accommodation of G-series Nerve Agents and HI-6 by hAChE

In order to fully understand how structural variations, between G-series agents, impacts the ability to reactivate hAChE, multiple structures of inhibited-hAChE in complex with HI-6 were created and analyzed. Each G-series nerve agent-inhibited hAChE's HI-6 shared similar conformations at first glance. Additionally, these structures shared two similar conformations within the PAS site, due to the known flexibility of Trp286 and its ability to exhibit significant conformational changes to accommodate such oximes. Considering GA and GB-inhibited hAChE, the tail-end of HI-6 forms hydrogen bond interactions with either Glu285 or with S298 depending on its conformation, while GD-inhibited hAChE's HI-6 forms hydrogen bonds with Val282. These tail-end interactions create a stabilizing force on the back end of HI-6 allowing it structural support

for entrance into the active site. All-inclusive, these varying positions of the PAS site do not propose any novel relevant information to G-series inhibition structural components due to the nature of Trp286. Fortunately, similar overall spatial arrangements of HI-6 within G-series agent-inhibited hAChE have been observed with VX-inhibited hAChE as HI-6_1 and HI-6_3 and this previous research demonstrated that these conformations of HI-6 are considered 'productive' poses and contain the potential for reactivation.[13]

Travelling along HI-6, depending on the inhibitor present and conformation of HI-6, the linker oxygen can make possible hydrogen bond interactions with Tyr124, although not very strong due to the length of the bond. This bond is only observed within GB-inhibited hAChE, potentially because HI-6 is able to move deeper into the active site relative to GA/GD-inhibited hAChE's HI-6, bringing the linker oxygen closer to Tyr124 and stabilizing it. Further along HI-6, the nitrogen within the second pyridinium ring of HI-6 makes hydrogen bond interactions. GD and GB-inhibited hAChE HI-6 utilizes Tyr124 to form hydrogen bond interactions with this nitrogen. GD's HI-6 forms a shorter bond compared to GB's HI-6 due to GB's HI-6 travelling further into the active site and distancing its nitrogen from the Tyr124. When analyzing GA-inhibited hAChE's HI-6, no hydrogen bonds are formed between this nitrogen and HI-6. Due to GA's orientation, it appears that because Phe295 is shifted outward of the active site, causing Val294 and Arg296 to follow suit, HI-6 has more space inside the active site to move freely. This extra empty area potentially causes HI-6 to travel into the active site with less of a direct route and lose a stabilizing interaction with Tyr124.

The bonds formed deepest into the active site rely on the orientation of HI-6's oxime arm. In both conformations of GA-inhibited hAChE, HI-6's nitrogen within its

oxime arm forms hydrogen bond interactions with Tyr124 and a nearby water while its oxygen forms hydrogen bonds with that nearby water as well. When analyzing GD-inhibited hAChE, its HI-6's oxime arm makes similar hydrogen bond interactions with Tyr124 and a nearby water in a very similar spatial arrangement with distance slightly varying. Naturally, GB-inhibited hAChE's HI-6 creates vastly different interactions with its oxime arm due to the arm being rotated ~180° clockwise relative to GA and GD's HI-6. It appears that because of GB-inhibited hAChE's HI-6 is deeper into the active site, its oxime arm would potentially form long and unstable bonds if in a similar conformation as GA/GD-inhibited hAChE. Therefore, it finds another option, Val294, and uses this for stabilization.

The overall spatial arrangements of each HI-6 and their ability to reactivate, appear to rely on their distance into the active site. Generally, the closer HI-6 is to the active site and inhibitor the more likely it is to reactivate due to the oxime arm interactions being in closer proximity. When comparing each G-series-inhibited hAChE's HI-6, GB-inhibited hAChE allowed its HI-6 to further travel into the active site. One of the main deciding factors in this movement appear to be the spatial orientation of Tyr337. While GA-inhibited hAChE's Tyr337 is further downward and GD-inhibited hAChE's Tyr337 is further downward and leftward, GB-inhibited hAChE's Tyr337 is relatively higher than the others. It appears that the movement of Tyr337 stem from the particular inhibitor present. With GD's bulky carbonous side group, it likely sterically hinders Tyr337 forcing it away from the inhibitor and potentially blocking HI-6's pathway into the active site. Similar HI-6 blockage originates from GA-inhibited hAChE's Tyr337, where instead of steric hindrance, hydrophobic interactions between the ethoxy side group and Tyr337 appear to

form. Naturally, GB-inhibited hAChE's HI-6 is allowed deeper access into the active site. Its Tyr337 does not appear to be sterically hindered nor forming hydrophobic interactions, due to its 'Y' shaped side group lacking both possibilities. Other residues within inhibited-hAChE further support Tyr337's role in active site depth and the stabilization of HI-6 wherever it may orient itself. Depending on the spatial arrangement of HI-6, it appears that both Tyr341 and Tyr124 make modifications to ensure their stabilizing interactions with HI-6. Due to GB-inhibited hAChE's HI-6, Tyr 341 is shifted the furthest upward relative to GA/GD-inhibited hAChE. This shift allows for optimal stacking between the second pyridinium ring of HI-6 and Tyr341. Additionally, Tyr124 is pushed closed into the active site to confirm t-shaped stacking. While observing GA-inhibited hAChE, its Tyr341 is moved slightly toward Phe295 to accommodate HI-6's spatial arrangement within the active site for stacking and Tyr124 is also shifted towards Phe295 to further secure t-shaped stacking for stabilization. Accordingly, GD-inhibited hAChE follows this trend to stabilize its HI-6 in the active site having the lowest spatial orientation of Tyr341 and a Tyr124 further away from Phe295 than the Tyr124 of GA-inhibited hAChE. It appears that Tyr341 reacts to the spatial arrangements of the particular G-series nerve agent present in the active site, which potentially causes conformational changes to the following residues in order to accommodate HI-6.

Materials and Methods

Materials

Acetylthiocholine, 5,5'bis-dithio-2-nitrobenzene (DTNB), HI-6, sodium carbonate, monosodium phosphate and disodium phosphate were purchased from Sigma-Aldrich (St. Louis, MO USA). HEPES, KNO3, PEG-3350 solutions purchased from Hampton Research, Aliso Viejo, CA Laboratory deionized water > 17 MΩ was used for all assays. Hexane and isopropyl alcohol were purchased from Fisher Scientific (Waltham, MA).

Cloning, Expression, and Purification of hAChE

Expression and purification of hAChE was as previously described[21, 25, 26] by transfecting recombinant octahistidine (His_8)-tagged hAChE amino acid sequence 1-574 (pre-processed protein numbering which includes the native secretion signal) encoded construct into HEK-293-H cells (Invitrogen). Purified protein was dialyzed into storage buffer C (10 mM HEPES pH 7.0, and 10 mM NaCl) overnight and concentrated to 16 mg/ml for crystallization.

Measurement of inhibition rate constants

All procedures in regard to measurement of reactivation rate constants were adapted from previously described methods[13]. Inhibited hAChE was prepared by diluting AChE into 50 µL of 50 mM phosphate buffer, pH 8.0 containing BSA (5%), and 10 µL of GA/GB/GF/GP (1 mg/mL), incubated on ice for 30 min, then remove excess inhibitor by centrifugation through a Centri-Sep spin column, at 750xG for 2 min, prior to dilution in the same buffer (pH 8.0 containing 0.1 mg/ml BSA), aliquoted (900 µL), and stored at –80 °C. The same modified Ellman's assay as for determining the inhibition kinetics of GA and

GB was utilized to observe reactivation kinetics of HI-6. Briefly, the assay solution was dispensed via the plate reader into 96-well flat-bottomed polystyrene microplate containing the desired concentration of reactivator. Reactivation of inhibited AChE was determined by adding a reactivator (1500, 1000, 500, 250, 150, or 15 µM, final concentration) to the GA/GB/ (and 1500, 1000, 750, 600, 500, 375, 300, 250, 200, 125, 50, or 25 µM) GP/GF inhibited AChE immediately prior to inserting into the plate reader. The activity measured at 30 s, 1, 2, 3, 4, 5, and 30 min. k_2 is the intrinsic reaction constant; K_{OX} is the apparent equilibrium constant; and k_r is the second-order reactivation rate constant [11]. The change in percent reactivated AChE was proportional to the rate of hydrolysis of acetylthiocholine relative to uninhibited AChE. The rate of reactivation (k_{obvs}) at each concentration is given by equation 1, which assumes complete inhibition. All experiments were performed in triplicate.

Measurement of reactivation rate constants

All procedures in regard to measurement of reactivation rate constants were adapted from previously described methods[13]. Inhibited hAChE was prepared by diluting AChE into 50 µL of 50 mM phosphate buffer, pH 8.0 containing BSA (5%), and 10 µL of GA/GB/GF/GP (1 mg/mL), incubated on ice for 30 min, then remove excess inhibitor by centrifugation through a Centri-Sep spin column, at 750xG for 2 min, prior to dilution in the same buffer (pH 8.0 containing 0.1 mg/ml BSA), aliquoted (900 µL), and stored at –80 °C. The same modified Ellman's assay as for determining the inhibition kinetics of GA and GB was utilized to observe reactivation kinetics of HI-6. Briefly, the assay solution was dispensed via the plate reader into 96-well flat-bottomed polystyrene microplate containing the desired concentration of reactivator. Reactivation of inhibited AChE was determined

by adding a reactivator (1500, 1000, 500, 250, 150, or 15 μM, final concentration) to the GA/GB/GF/GP inhibited AChE immediately prior to inserting into the plate reader. The activity measured at 30 s, 1, 2, 3, 4, 5, and 30 min. k_2 is the intrinsic reaction constant; K_{OX} is the apparent equilibrium constant; and k_r is the second-order reactivation rate constant [11]. The change in percent reactivated AChE was proportional to the rate of hydrolysis of acetylthiocholine relative to uninhibited AChE. The rate of reactivation (k_{obvs}) at each concentration is given by equation 1, which assumes complete inhibition. All experiments were performed in triplicate.

Human acetylcholinesterase crystallization and inhibitor soaking

Crystallization of hAChE for ligand soaks occurred following the general procedures communicated in recent studies [21, 27]. In short, purified protein concentrated to 16 mg/mL and apo hAChE crystals were grown by sitting drop vapor diffusion at 22°C against 5 μL crystallization buffer. The crystallization buffer contained 15-21% polyethylene glycol 3350 (PEG) and 0.17-0.21 M potassium nitrate. The hexagonal rod-shaped crystals generally nucleated within 5 days and finished their growth after an additional 3 days. Crystals of a ligand in complex with hAChE were obtained by soaking apo crystals at 22°C in crystallization buffer accompanied by 20-25% ethylene glycol and specific concentrations of each ligand for individually designated periods of time. To obtain the AChE-GA-HI-6 complex, the crystal was soaked in 24.67 mM GA for 1 minute and an 11.1 mM HI-6 solution for 1 minute. For the AChE-GB-HI-6 complex, the apo crystals were soaked in buffer with a concentration of 28.55 mM GB for 2 minutes and then buffer with 11.1 mM concentration of HI-6 for 2 minutes. For the AChE-GD-HI6 complex, the apo crystals were soaked in buffer with a concentration of 24.67 mM GD for

2 minutes and then buffer with 11.1 mM concentration of HI-6 for 2 minutes. The crystals were then mounted onto liquid nitrogen flash-cooled nylon loops. To obtain AChE-GA, the AChE crystal was soaked in 6.17 mM GA for 7 minutes. To obtain AChE-GB, the AChE crystal was soaked in 42.83 mM GA for 1 minutes. To obtain AChE-GD, the AChE crystal was soaked in 10 mM GA for 1 minutes. To obtain AChE-GF, the AChE crystal was soaked in 33.3 mM GF for 30 minutes and to achieve AChE-GP, the AChE crystal was soaked in 10 mM for 2 minutes.

Data collection, reduction, and refinement

Data sets were collected for AChE-GA and AChE-GA-HI-6 with a resolution of 2.63 Å and 2.46 Å respectively on the 22ID beamline of SERCAT at the Advanced Photon Source, Argonne National Laboratory using a monochromic X-ray beam with a Rayonix (Mar) 300HS high speed CCD detector. Data sets were collected for AChE-GB-HI-6 and AChE-GB complexes with a resolution of 2.37 Å and 2.25 Å respectively on the 22BM beamline of SERCAT at the Advanced Photon Source, Argonne National Laboratory using a monochromic X-ray beam with a Mar300 CCD detector. Data sets were collected for AChE-GD and AChE-GD-HI-6 with a resolution of 2.63 Å and 2.46 Å respectively on the 22ID beamline of SERCAT at the Advanced Photon Source, Argonne National Laboratory using a monochromic X-ray beam with a Rayonix (Mar) 300HS high speed CCD detector. Data sets were collected for AChE-GF and AChE-GP with a resolution of 2.31 Å and 2.30 Å respectively on the 22ID beamline of SERCAT at the Advanced Photon Source, Argonne National Laboratory using a monochromic X-ray beam with a Rayonix (Mar) 300HS high speed CCD detector. X-ray images were indexed, strategized, integrated, and scaled processed, using HKL2000 [28]. CCP4 software suite was employed to create a cross-

validation set from a random 5% of the reflections and the same test set was employed throughout the structural refinement [29]. The initial phase solutions for the structures were established using molecular replacement via Phaser with 4EY4 [21] as an initial mode [30]. The refinement of the structures was performed using repetitive cycles of model building and refinement using COOT and Phenix to refine respectively. TLS Motion Determination (TLSMD) was utilized to analyze the structure for flexibility and this analysis was employed for TLS parameters in Phenix Refine to aid in refining anisotropic displacements in the structures [31]. Water molecules were originally added to $2F_o$ - F_c density peaks of greater than 1σ using Find Water COOT program function and then were assessed individually [32]. Subsequently, carbohydrates, PEGs, and other ligands were individually placed into structures based on $F_o – F_c$ density at 3σ and refined with Phenix.Refine after which the structures are positioned to fit the $2F_o – F_c$ density at 1σ. The final model of each structure was examined via Molprobity to confirm the quality of the structures. The data collection and refinement statistics for each structure are listed in Table 2.2.

Tables

Table 2.1. a. Inhibition and b. Reactivation of hAChE

a.	OP	k_2 (min^{-1})	K_d (M)	k_i (M^{-1} min^{-1})
	GB	1.6×10^{-02}	1.4×10^{-09}	$1.1 \times 10^{+07}$
	GA	2.4×10^{-02}	1.0×10^{-08}	$2.3 \times 10^{+06}$
	GF	3.0×10^{-02}	6.5×10^{-11}	$4.6 \times 10^{+08}$
	GP	2.5×10^{-02}	2.9×10^{-09}	$8.9 \times 10^{+06}$
	GD	1.6×10^{-02}	3.6×10^{-10}	$4.4 \times 10^{+07}$

b.	OP	k_2 (min^{-1})	K_{OX} (µM)	k_r (µM^{-1} min^{-1})	max %
	(±)-GA	3.50 ± 0.65	0.75 ± 5.6	4.65 ± 34.6	7
	(±)-GB	1.07 ± 0.08	23.8 ± 6.0	0.045 ± 0.010	>100
	(±)-GF	.130 ± .009	40.30 ± 10.34	.0032 ± .0013	>100
	C(+)P()-soman[a]	n.c.*	n.c.*	n.c.*	676 (6)
	C(-)P()-soman[a]	n.c.*	n.c.*	n.c.*	23 4 (8)

n.c. refers to non-calculable.

[a]*de Jong's data*[10]

Table 2.2 Crystallography Data of hAChE Structures

a. (PDB)	AChE-GA	AChE-GB	AChE-GD	AChE-GF	AChE-GP
Data collection					
space group	$P3_121$	$P3_121$	$P3_121$	$P\ 3_1\ 2\ 1$	P 31 2 1
cell dimensions					
a, b, c (Å)	104.5, 104.5, 323.8	104.9, 104.9, 323.3	105.1, 105.1, 323.7	105, 105, 324	105.1, 105.1, 323.3
a, b, g (°)	90, 90, 120	90.0, 90.0, 120.0	90, 90, 90	90, 90, 120	90, 90, 120
resolution (Å)	50.0 – 2.63 (2.68 - 2.63)[a]	50-2.25 (2.29-2.25)[a]	50.0 – 2.60	50.0 – 2.3 (2.35 - 2.31)	50.0 - 2.3 (2.37 - 2.29)
completeness (%)	99.0 (99.3)[a]	96.7 (75.2)[a]	100.0 (100.0)[a]	99.6 (93.7)	100.0 (99.9)
R_{merge} (%)[b]	9.8 (74.7)[a]	8.3 (51.9)[a]	11.7 (59.4)[a]	8.4 (46.1)	
R_{pim} (%)	6.0 (47.6)[a]	3.5 (25.9)[a]	4.7 (23.8)[a]	4.0 (23.1)	
CC 1/2	(0.661)[a]				
I/σ	11.4 (2.1)[a]	29.9 (2.72)[a]	15.8 (2.9)[a]	15.6 (3.8)	20.3 (2.9)
redundancy	3.6 (3.4)[a]	6.5 (4.4)[a]	7.1 (7.2)[a]	5.3 (4.9)	7.2 (5.4)
Refinement					
resolution (Å)	37.5 – 2.63 (2.74-2.63)	40.74-2.253 (2.33-2.25)	46.1 – 2.6	40 – 2.3 (2.4-2.3)	45.5 - 2.3
no. reflections	61463 (5861)	95284	64893	91118 (8975)	94100
R_{work} (%)[c]/R_{free} (%)[c]	17.6/20.8	16.82/19.00	15.5/19.7	17.2/20.2	16.4/20.0
no.atoms (protein/ligand/water)	8369/172/272	8347/149/896	8377/131/959	8357/128/508	8421/192/814
B-factors					
protein	65.7	36.93	49.5	41.6	42.7
ligands	117.7	91.40	86.0	73.0	82.5
Water	67.8	49.80	58.4	46.0	49.7
Deviations					
bond lengths (Å)	0.018	0.005	0.01	0.019	.008
bond angles (°)	1.31	0.83	1.02	1.98	1.29

b.	AChE GA-HI-6	AChE GB-HI-6	AChE GD-HI-6 (
Data collection			
space group	$P3_121$	$P3_121$	$P3_121$
cell dimensions			
a, b, c (Å)	105.3, 105.3, 324.9	104.2, 104.2, 323.8	104.9, 104.9, 322.8
a, b, g (°)	90.0, 90.0, 120.0	90.0, 90.0, 120.0	90.0, 90.0, 120.0
resolution (Å)	50.0 – 2.46 (2.50-2.46) [a]	50.0 – 2.37 (2.41 - 2.37) [a]	200.0 - 2.20 (2.24 - 2.20) [a]
completeness (%)	99.8 (99.4) [a]	99.5 (100.0) [a]	100.0 (100.0) [a]
R_{merge} (%)[b]	7.1 (63.9) [a]	6.9 (34.3) [a]	
R_{pim} (%)	3.1 (30.6) [a]	4.2 (21.8) [a]	
CC 1/2=	(0.896) [a]		
I/σ	17.5 (2.1) [a]	17.4 (3.9) [a]	10.7 (0.57) [a]
redundancy	6.0 (5.2) [a]	3.3 (3.2) [a]	9.2 (9.3) [a]
Refinement			
resolution (Å)	41.36 – 2.45 (2.54 – 2.45)	37.01 – 2.37 (2.46 - 2.37)	49.87 – 2.19 (2.27 – 2.19)
no. reflections	77311	83122 (8105)	106317 (10388)
R_{work} (%)[c]/R_{free} (%)[c]	19.02/22.10	17.6/21.1	19.7/23.3
no. atoms (protein/ligand/water)	8318/211/397	8374/202/586	8431/214/515
B-factors			
protein	65.4	48.17	45.27
ligands	108.9	90.01	66.08
Water	66.5	56.58	48.24
Deviations			
bond lengths (Å)	0.012	0.004	0.009
bond angles (°)	1.20	0.717	1.20

[a]Data for the last resolution shell are provided in parentheses. [b]Rmerge =ΣhΣI|II(h) − ⟨I(h)⟩|/ΣhΣiII(h), where II(h) is the ith measurement and ⟨I(h)⟩ is the weighted mean of all measurements of I(h). [c]Rwork and Rfree = h[|F(h)obs| − |F(h)calc|]/h|F(h)obs| for reflections corresponding to the working and test sets.

Figures

Figure 2.1. Chemical structures of organophosphate nerve agents. The chemical structure of OP nerve agents with colored labels corresponding to either the V-series (green), G-series (blue) or Novichok (red) class.

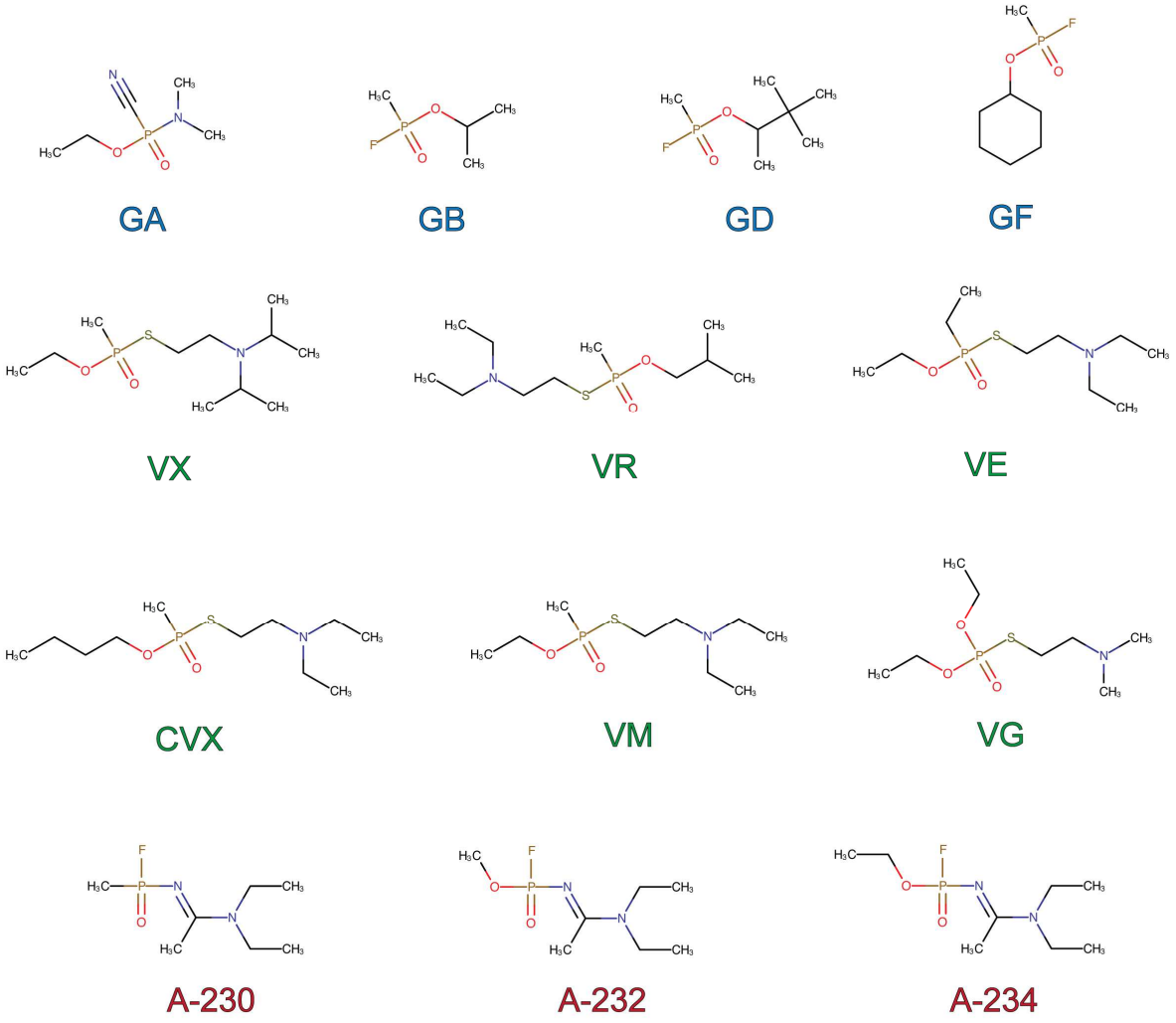

Figure 2.2. Chemical structures of common oxime-based therapeutic reactivators.

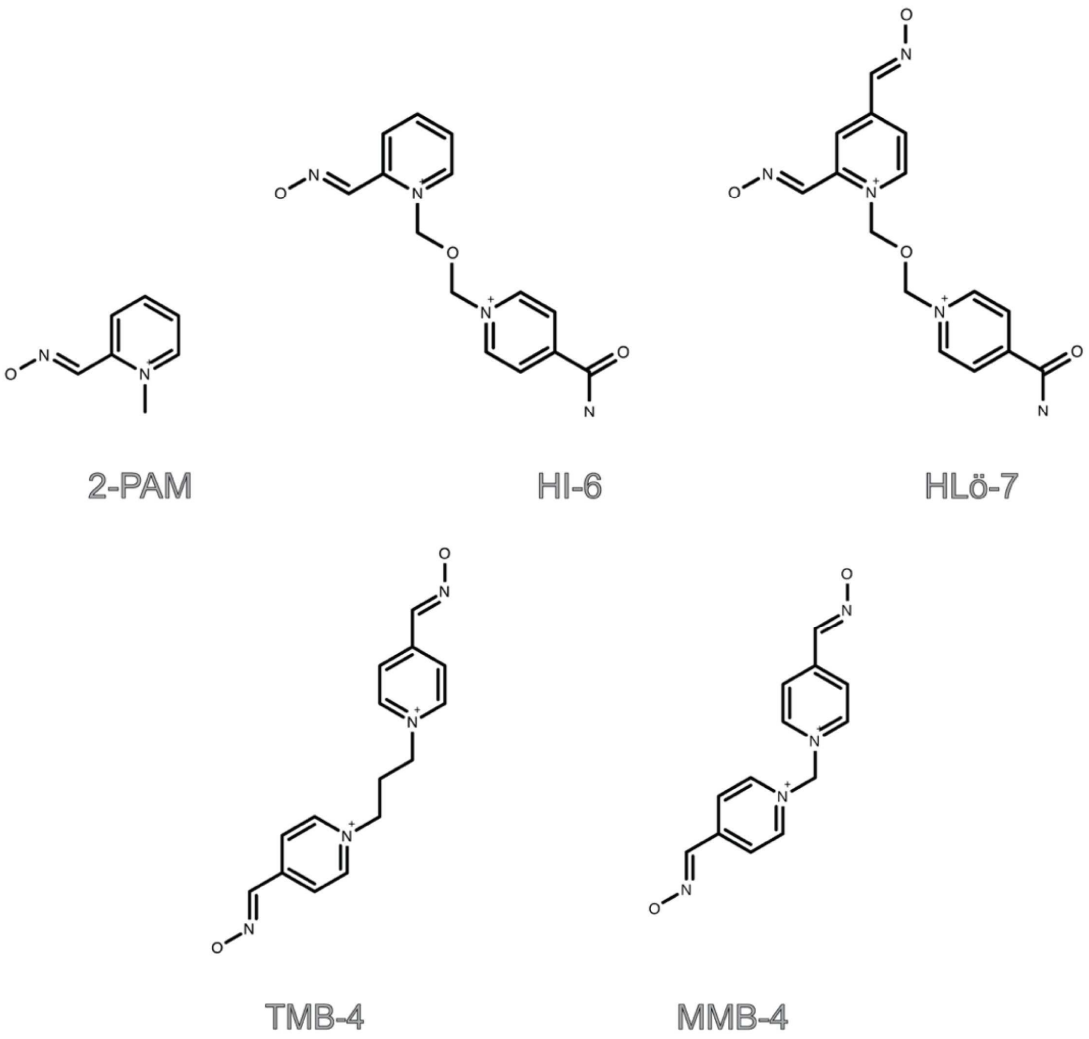

Figure 2.3. Crystal structures of human acetylcholinesterase in complex with different G-series nerve agents. (a) Structure of GA (salmon) bound to the active site of hAChE (pale cyan) (b) Structure of GB (dark violet) bound to the active site of hAChE (blue-grey). (c) Structure of GD (silver) bound to the active site of hAChE (pale green) . (d) Structure of GF (maroon) bound to the active site of hAChE (yellow). (e) Structure of GP (dark grey) bound to the active site of hAChE (light orange). The black dashes represent hydrogen bonds. AChE residues are represented by black letters, while the red letters are the distances (Å).

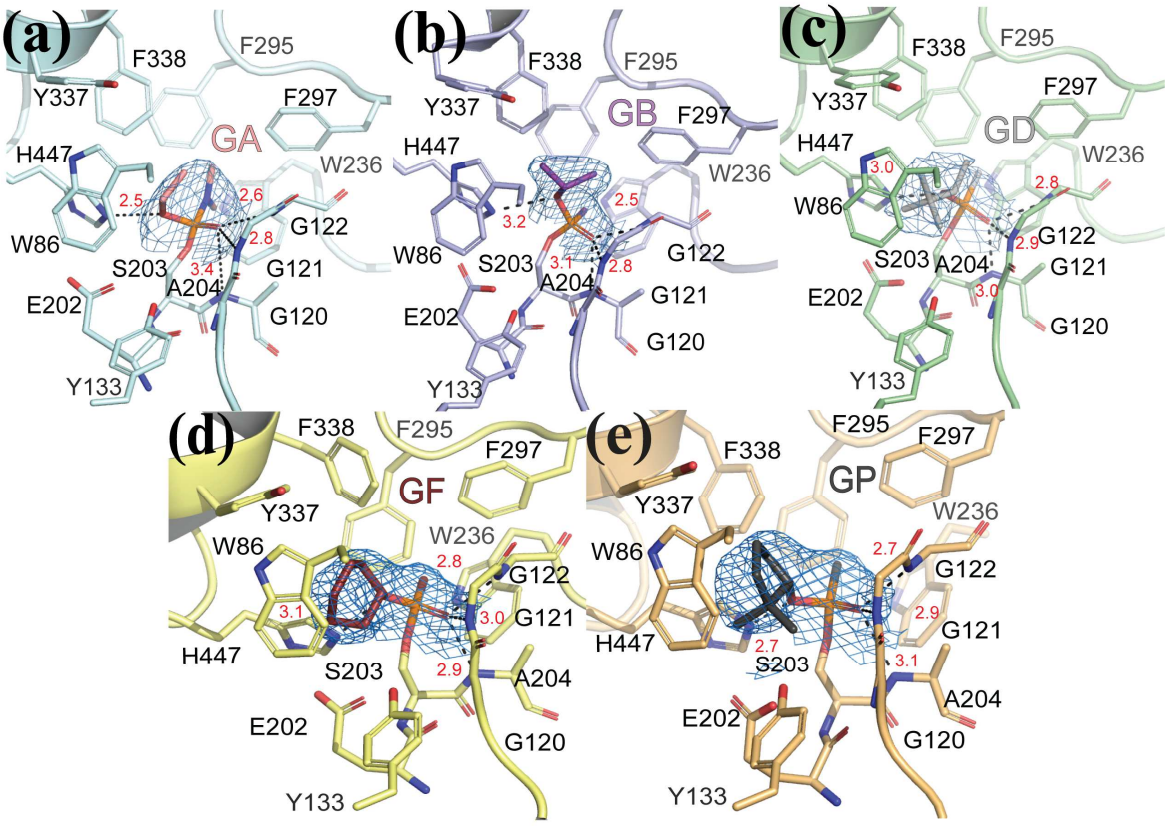

Figure 2.4. Crystal structures of human acetylcholinesterase in complex with different G-series nerve agents. Wall-eyed stereo view of GA (salmon), GB (dark violet), and GD (silver) -inhibited hAChE (pale cyan, blue-grey, and pale green respectively). AChE residues are represented by black letters.

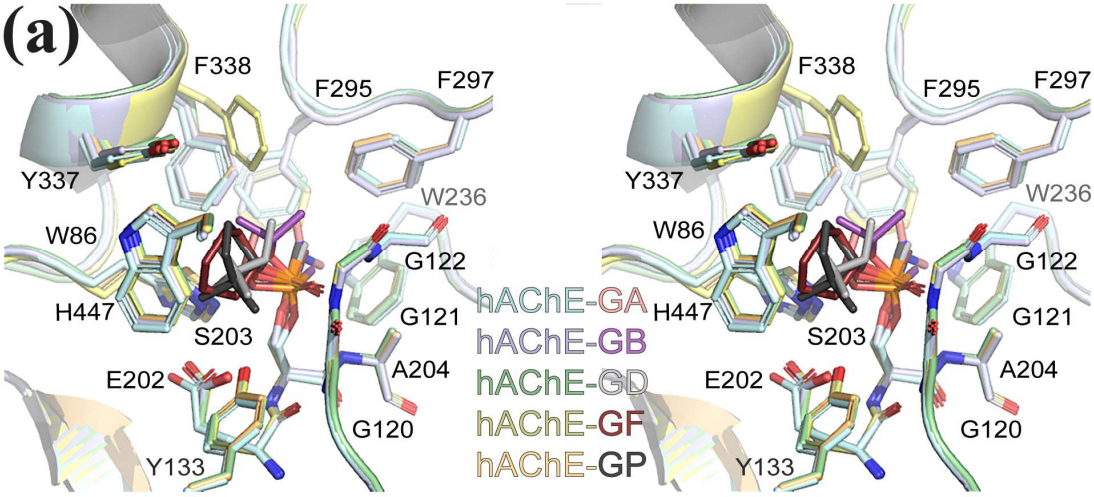

Figure 2.5. Crystal structures of human acetylcholinesterase in complex with different G-series nerve agents. Structures of GA (salmon), GB (dark violet), GD (silver), GF (dark red), and GP (dark grey) -inhibited hAChE (pale cyan, blue-grey, pale green, light yellow, and light orange respectively). The black dashes represent hydrogen bonds. AChE residues are represented by black letters, while the red letters are the distances

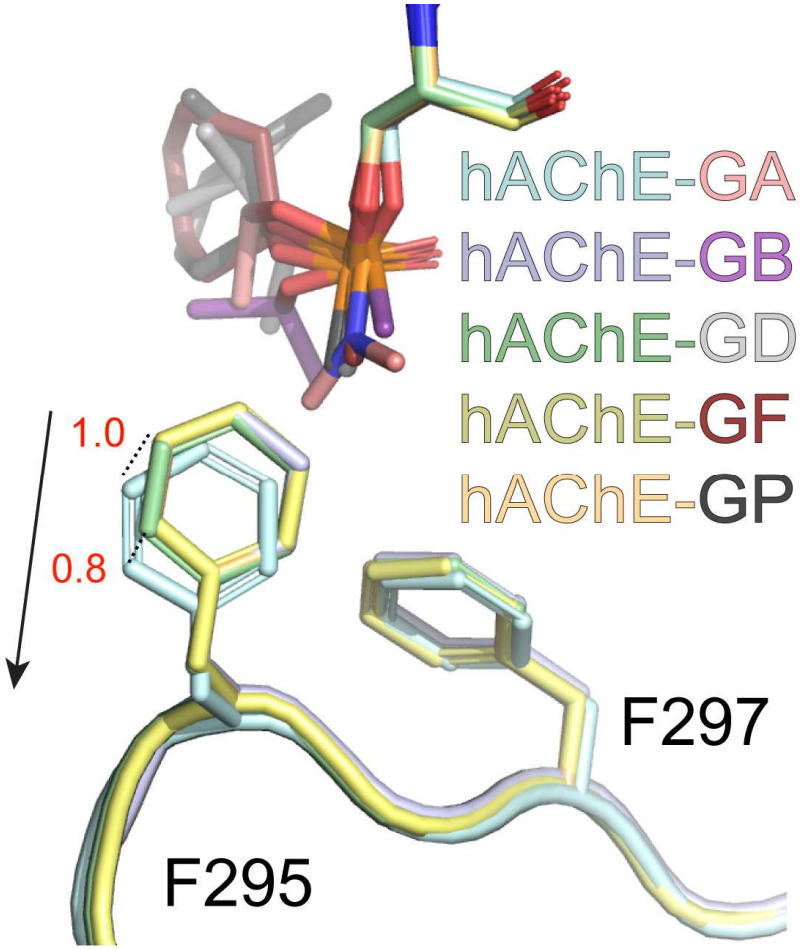

Figure 2.6. Crystal structures of human acetylcholinesterase in complex with different G-series nerve agents as well as reactivator HI-6. (a/b) Two conformations of HI-6 (orange and pale yellow) in complex with GA (salmon)-inhibited hAChE (grey-green). (c/d) Two conformations of HI-6 (light teal and dark teal) in complex with GB (dark violet)-inhibited hAChE (light pink). Structure of HI-6 (dark red) in complex with GD (silver)-inhibited hAChE (wheat). Waters are shown as red spheres. The black dashes represent hydrogen bonds. AChE residues are represented by black letters, while the red letters are the distances (Å).

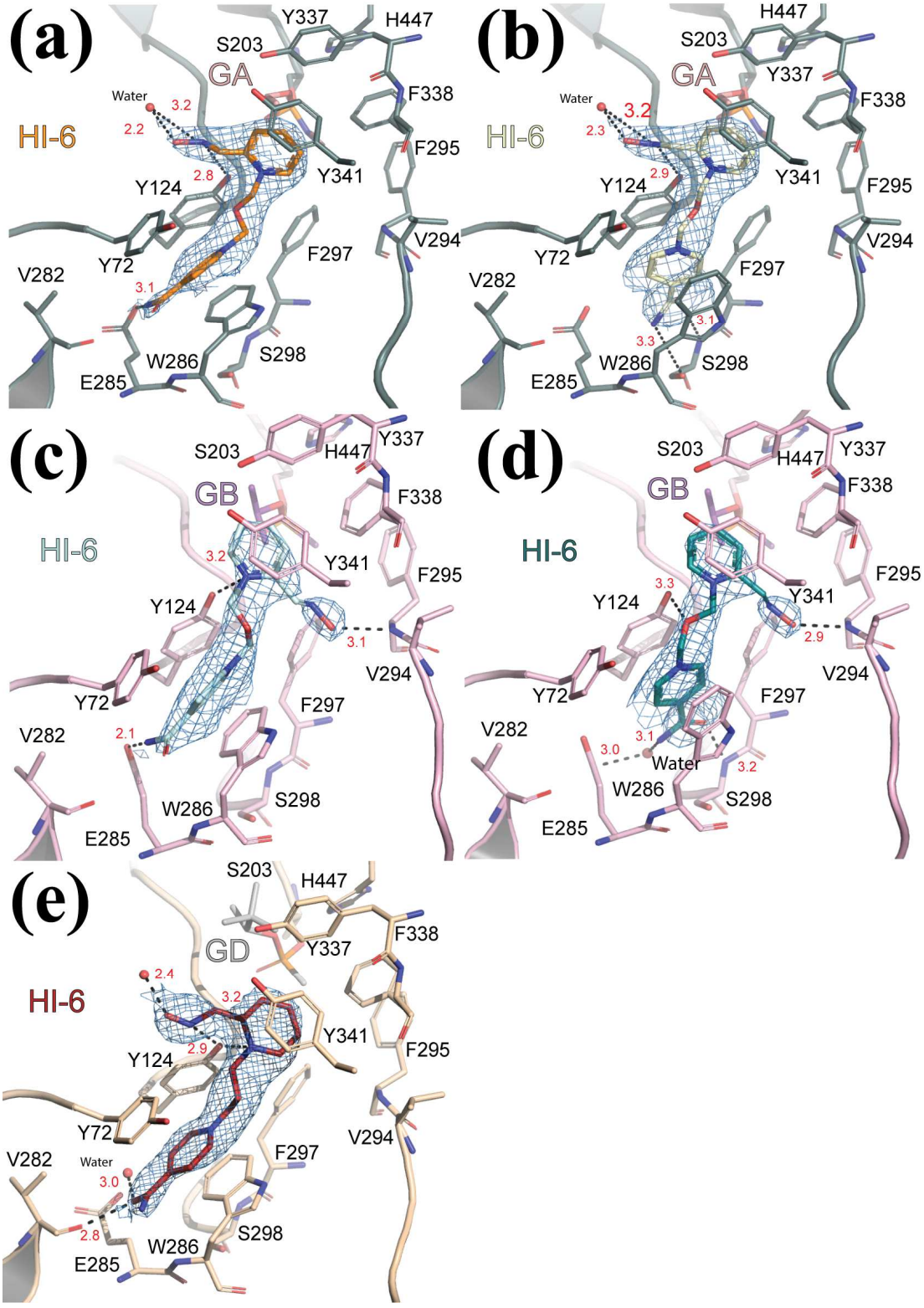
(a)
GA
HI-6
Water
3.2
2.2
2.8
3.1
Y337
H447
S203
F338
F295
Y341
Y124
F297
V294
Y72
V282
W286
S298
E285
(b)
GA
HI-6
Water
3.2
2.3
2.9
3.1
3.3
H447
S203
Y337
F338
F295
Y341
Y124
V294
Y72
F297
V282
W286
S298
E285
(c)
GB
HI-6
3.2
3.1
2.1
S203
H447
Y337
F338
Y341
F295
Y124
V294
Y72
F297
V282
W286
S298
E285
(d)
GB
HI-6
3.3
3.1
3.0
3.2
2.9
S203
H447
Y337
F338
F295
Y124
Y341
V294
Y72
F297
V282
Water
W286
S298
E285
(e)
GD
HI-6
2.4
3.2
2.9
2.8
3.0
S203
H447
F338
Y337
Y341
F295
Y124
Y72
V294
F297
V282
Water
S298
W286
E285

Figure 2.7. Crystal structures of human acetylcholinesterase in complex with different G-series nerve agents as well as reactivator HI-6. (a) Wall-eyed stereo view of GA (salmon), GB (dark violet), and GD (silver) -inhibited hAChE (grey-green, light pink, and wheat respectively) in complex with the first conformation of HI-6 (orange-GA, light teal-GB, and dark red-GD). (b) Wall-eyed stereo view of GA (salmon), GB (dark violet), and GD (silver) -inhibited hAChE (grey-green, light pink, and wheat respectively) in complex with the second conformation of HI-6 (pale yellow-GA, dark teal-GB, and dark red-GD) . AChE residues are represented by black letters.

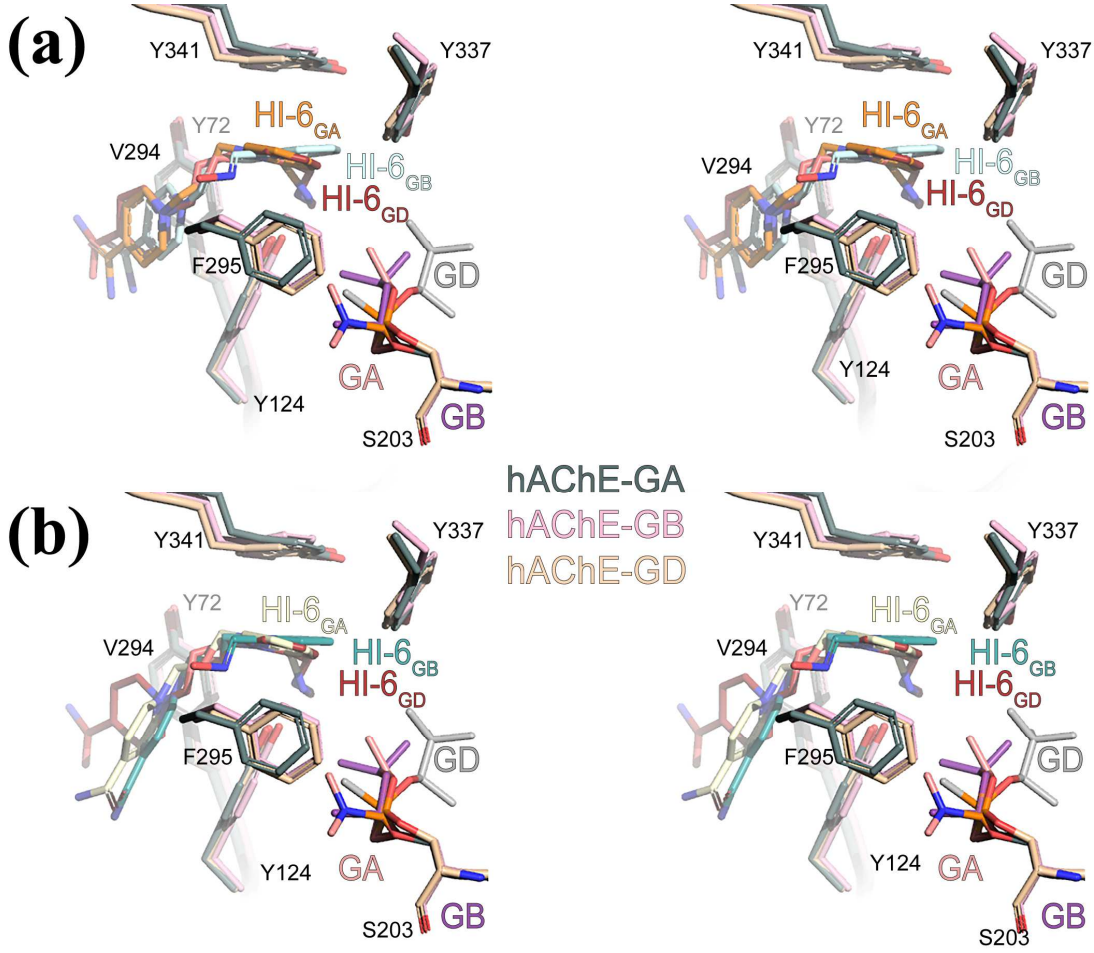

Figure 2.8. Inhibition, Aging, and Reactivation of G-series nerve agents in hAChE.

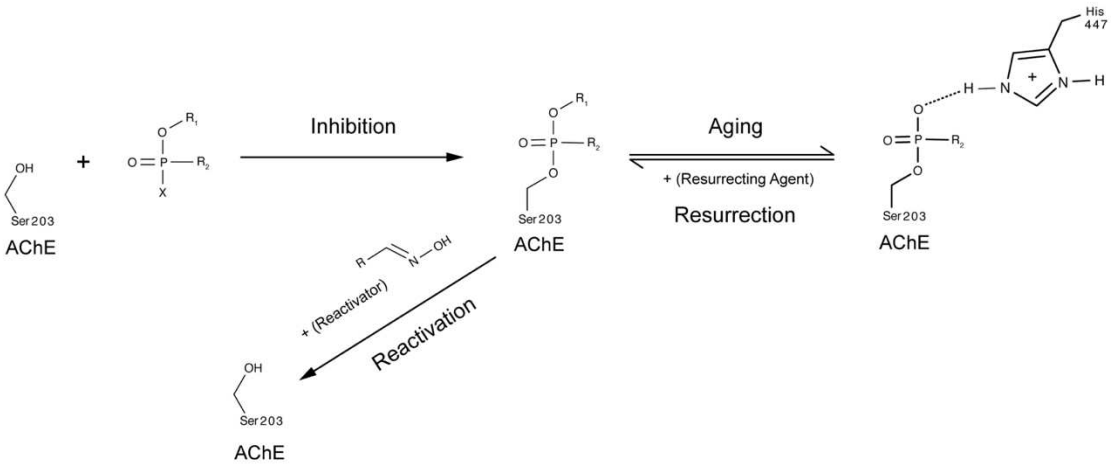

Associated Content

Supporting Information.

Additional figures illustrating G-series nerve agents inhibiting hAChE and/or in complex with HI-6 are available in Appendix A and B.

Author Information

Corresponding Author

*Correspondence addressed to College of Pharmacy University of Georgia, 422 Pharmacy South, Athens, GA 30602, or U.S. Army Edgewood Chemical Biological Center, Aberdeen Proving Ground, MD 21010-5424, USA. Tel: (706) 542 3435; spegan@uga.edu (SDP), or (410) 436 3460; jude.j.height.civ@mail.mil (JJH).

Author Contributions

The manuscript was written through contributions of all authors. All authors have given approval to the final version of the manuscript.

Funding Source

Use of the Advanced Photon Source was supported by the U.S. Department of Energy, Office of Science, Office of Basic Energy Sciences, under Contract W-31-109-Eng-38 (SDP). Data for structures were collected at Southeast Regional Collaborative Access Team (SER-CAT) 22-BM beamline at the Advanced Photon Source, Argonne National Laboratory. Supporting institutions may be found at www.ser-cat.org/members.html. Data for were collected on the 19-ID beamline at Structural Biology Center at the Advanced Photon Source. Argonne is operated by University of Chicago Argonne, LLC, for the U.S. Department of Energy, Office of Biological and Environmental Research under contract DE-AC02-06CH11357.

Notes

The authors declare no competing financial interest.

++ The atomic coordinates and structure factors have been deposited in the RCSB Protein Data Bank, www.rcsb.org.

Acknowledgements

This work funded by Defense Threat Reduction Agency project: CB#3889 "Elucidation of the mechanisms and physical properties of the molecular targets of chemical nerve agents" (JJH). Thanks to Dr. Steven Harvey for continuous advice on agent chemistry and agent kinetics throughout the project. Thanks to Dennis Bevilaqua and Nicole Rippeon.

Abbreviations used

AChE, acetylcholinesterase, (hAChE human and hAChE recombinant human); ALS, Advanced Light Source; CASARM, Chemical Agent Standard Analytical Reference Material; DTNB, 5,5'-dithio-bis(2-nitrobenzoic acid); TNB, 5-thio-2-nitrobenzoic acid; 2-PAM or pralidoxime, 2-[(hydroxyimino)methyl]-1-methylpyridin-1-ium; VX, Ethyl ({2-[bis(propan-2-yl)amino]ethyl}sulfanyl)(methyl)phosphinate;GA,tabun, dimethylamino(ethoxy)phosphoryl]formonitrile;GB,Sarin, 2-[fluoro(methyl)phosphoryl]oxypropane; GD, soman, 3,3-DImethylbutan-2-yl methylphosphononfluoridate; GF, cyclosarin, [fluoro(methyl)phosphoryl] oxycyclohexane;

REFERENCES

1. K. Ganesan, S.K.R., R. Vijayaraghavan, *Chemical warfare agents*. J pharm Bioallied Sci., 2010. **2(3)**: p. 166-178.
2. P., A., *The threat of mid-spectrum chemical warfare agents.* The threat of mid-spectrum chemical warfare agents., 2003. **18:306-12**.
3. Sidell, F.R., E.T. Takafuji, and D.R. Franz, *Medical Aspects of Chemical and Biological Warfare*, D.T.I. Center, Editor. 1997.
4. Paddock, R., C. Sang-Hun, and N. Wade, *In Kim Jong-nam's Death, North Korea Lets Loose a Weapon of Mass Destruction*, in *The New York Times*. 2017.
5. *Amesbury poisoning: Experts confirm substance was Novichok*, in *British Broadcasting Company*. 2018: Internet.
6. Kingsley, P. and A. Barnard *Banned Nerve Agent Sarin Used in Syria Chemical Attack, Turkey Says*. The New York Times, 2017.
7. *Note by the Technical Secretariat: Guidance for States Parties on Article VI Declaration Obligations and Inspections Following Entry into Force of Changes to Schedule 1 of the Annex on Chemicals to the Chemical Weapons Convention*, in *S/1821/2019*, P.C.W. O, Editor. 2020, Organisation for the Prohibition of Chemical Weapons Technical Secretariat: Online.
8. Topczewski, J.J., et al., *Reversible inhibition of human acetylcholinesterase by methoxypyridinium species.* Bioorg Med Chem Lett, 2013. **23**(21): p. 5786-9.

9. Topczewski, J.J. and D.M. Quinn, *Kinetic assessment of N-methyl-2-methoxypyridinium species as phosphonate anion methylating agents.* Org Lett, 2013. **15**(5): p. 1084-7.

10. Worek, F., et al., *Kinetic analysis of interactions between human acetylcholinesterase, structurally different organophosphorus compounds and oximes.* Biochem Pharmacol, 2004. **68**(11): p. 2237-48.

11. Luo, C., et al., *An in vitro comparative study on the reactivation of nerve agent-inhibited guinea pig and human acetylcholinesterases by oximes.* Biochemistry, 2007. **46**(42): p. 11771-9.

12. W. Leuzinger, A.L.B., E. Cauvin, *Acetylcholinesterase. II. Crystallization, absorption spectra, isoionic point.* Proc Natl Acad Sci U S A, 1968. **59(2)**: p. 620-623.

13. Bester, S.M., et al., *Structural insights of stereospecific inhibition of human acetylcholinesterase by VX and subsequent reactivation by HI-6.* Chem Res Toxicol, 2018.

14. Ekstrom, F., et al., *Crystal structures of acetylcholinesterase in complex with HI-6, Ortho-7 and obidoxime: structural basis for differences in the ability to reactivate tabun conjugates.* Biochem Pharmacol, 2006. **72**(5): p. 597-607.

15. Worek, F., N. Aurbek, and H. Thiermann, *Reactivation of organophosphate-inhibited human AChE by combinations of obidoxime and HI 6 in vitro.* J Appl Toxicol, 2007. **27**(6): p. 582-8.

16. Eddleston, M., *Patterns and problems of deliberate self-poisoning in the developing world.* QJM, 2000. **93**(11): p. 715-31.

17. Benschop, H.P., et al., *Isolation, anticholinesterase properties, and acute toxicity in mice of the four stereoisomers of the nerve agent soman.* Toxicol Appl Pharmacol, 1984. **72**(1): p. 61-74.

18. de Jong LP, V.M., Langenberg JP, Hagedorn I, Lo¨ffler M., *The bispyridinium-dioxime HLo¨-7: A potent reactivator for acetylcholinesterase inhibited by the stereoisomers of tabun and soman.* Biochem Pharmacol., 1989. **15**(38(4)): p. 633-40.

19. Worek, F., H. Thiermann, and T. Wille, *The oximes HI-6 and MMB-4 fail to reactivate soman-inhibited human and guinea pig AChE: A kinetic in vitro study.* Toxicology Letters, 2018. **293**: p. 216-221.

20. Pohanka, M., et al., *Assessment of acetylcholinesterase activity using indoxylacetate and comparison with the standard Ellman's method.* Int J Mol Sci, 2011. **12**(4): p. 2631-40.

21. Cheung, J., et al., *Structures of human acetylcholinesterase in complex with pharmacologically important ligands.* J Med Chem, 2012. **55**(22): p. 10282-6.

22. Hornberg, A., A.K. Tunemalm, and F. Ekstrom, *Crystal structures of acetylcholinesterase in complex with organophosphorus compounds suggest that the acyl pocket modulates the aging reaction by precluding the formation of the trigonal bipyramidal transition state.* Biochemistry, 2007. **46**(16): p. 4815-25.

23. Artursson, E., et al., *Catalytic-site conformational equilibrium in nerve-agent adducts of acetylcholinesterase: possible implications for the HI-6 antidote substrate specificity.* Biochem Pharmacol, 2013. **85**(9): p. 1389-97.

24. Ekstrom FJ, A.C., Pang Y. , *Novel nerve-agent antidote design based on crystallographic and mass spectrometric analyses of tabun-conjugated acetylcholinesterase in complex with antidotes.* Clin Pharmacol Ther, 2007. **82**: p. 282-293.

25. Bester, S.M., et al., *The structural and biochemical impact of monomerizing human acetylcholinesterase.* Protein Sci, 2019.

26. Kronman, C., et al., *Production and secretion of high levels of recombinant human acetylcholinesterase in cultured cell lines: microheterogeneity of the catalytic subunit.* Gene, 1992. **121**(2): p. 295-304.

27. Franklin, M.C., et al., *Structures of paraoxon-inhibited human acetylcholinesterase reveal perturbations of the acyl loop and the dimer interface.* Proteins, 2016. **84**(9): p. 1246-56.

28. Otwinowski, Z. and W. Minor, *Processing of X-ray Diffraction Data Collected in Oscillation Mode*. Methods in Enzymology, ed. J. C.W. Carter and R.M. Sweet. Vol. 276: Macromolecular Crystallography, Part A. 1997, New York: Academic Press. 307-326.

29. Winn, M.D., et al., *Overview of the CCP4 suite and current developments.* Acta Crystallogr D Biol Crystallogr, 2011. **67**(Pt 4): p. 235-42.

30. McCoy, A.J., et al., *Phaser crystallographic software.* J Appl Crystallogr, 2007. **40**(Pt 4): p. 658-674.

31. Adams, P.D., et al., *PHENIX: a comprehensive Python-based system for macromolecular structure solution.* Acta Crystallogr D Biol Crystallogr, 2010. **66**(Pt 2): p. 213-21.

32. Emsley, P. and K. Cowtan, *Coot: model-building tools for molecular graphics.* Acta Crystallogr D Biol Crystallogr, 2004. **60**(Pt 12 Pt 1): p. 2126-32.

CHAPTER 3

DISCUSSION

Throughout history, the usage of chemical warfare has dealt devastating blows to populations and militaries on numerous occasions. Even today, the threat of the potential release of nerve agents or other chemical warfare is real. The threat of nerve agents is not something extremely new, however the therapeutics available to combat their inhibition are lacking. Diligent research concerning the structural underpinnings behind nerve agents and their kinetic abilities is required to fully understand why some reactivators are effective while others are not. It has been demonstrated that the impact a particular nerve agent produces within the active site of hAChE will ultimately impact the possibility of reactivation. The G-series family of nerve agents further supports this, however the mechanism behind these differences was unknown. In order to uncover the innerworkings of the G-series agents, further research was required.

Understanding G-series

To understand the unique interactions produced between G-series nerve agents and hAChE, x-ray crystallization was utilized. High-resolution structures allowed for highly accurate observation of hAChE inhibited by different nerve agents. At first glance, the G-series nerve agents appear to bind similarly to one another. With further analyzation, there is a noticeable shift in Phe295 within GA-inhibited hAChE and Phe338 in GF-inhibited hAChE. Unsurprisingly, this Phe295 shift was demonstrated in VX-inhibited hAChE resulting in an impact on its k_i. Previous studies additionally

demonstrated that tabun is extremely difficult to reactivate, which made this Phe295 shift even more interesting. In previous structures, inhibitors with large side groups pointed towards Phe295 cause a similar shift. For one, hAChE accommodates the more toxic enantiomer of VX with a shift in Phe295. Intriguingly, tabun is not composed of a large side group, instead it contains a smaller nitrogenous side group producing a similar shift. It appears that the electrostatic conditions exhibited by this side group are causing a shift in Phe295. Within VX-inhibited hAChE, the accommodations made by the active site hinder VX from making a hydrogen bond between His447 and its ethoxy side group. This deprives His447 from drawing electrons from the phosphorous atom of VX, making it more difficult for a potential nucleophilic attack from a reactivator. Interestingly, GA-inhibited hAChE still exhibits this bond between His447 and its side group. It appears that because of the extra electrons the nitrogenous group possesses, this His447 bond not only stabilizes tabun within the active site, but its pull of electrons required for the bond does not appear to lessen its resistance to reactivation. In addition to the significant shift in Phe295 the shift in Phe338 was something new, however reactivation of GF-inhibited hAChE was not previously studied. Therefore, its impact on the potential reactivation of hAChE was still unknown. Instead of causing difficult conformational and electrostatic changes within the active site like GA impacts Phe295, GF might have a favorable impact on the active site which allows Phe338 to conform to a more energetically favorable condition. To further understand the structural impact these nerve agents produced, inhibition kinetics were performed via Ellman's assays. As expected, GA-inhibited hAChE demonstrated a lower k_i than any other G-series agents, which further

supports the structural data due to the apparent steric hindrance. Additionally, GF had a relatively higher k_i which could stem from its Phe338 shift.

To continue the understanding of G-series interactions within the active site and tabun's resistance to reactivation, crystal structures containing the reactivator HI-6 were complexed with G-series-inhibited hAChE. Once again, the shift in Phe295 was demonstrated by GA-inhibited hAChE, which is exciting because of its conservation between just an inhibited structure to one with a reactivator. Other residues, including Tyr337, Tyr124, and Tyr341 appear to play a large role in the accommodation of HI-6 and hAChE's eventual reactivation. The structures of the nerve agents appear to play a significant role in the movement of Tyr337. Both GA and GD-inhibited hAChE allow Tyr337 to move further towards the agent which is potentially blocking HI-6's access to Ser203. The bulky carbonous side group of GD, pointed towards Tyr337 appears to cause a steric hindrance between the two and shifts Tyr337 towards HI-6 and downward. On the contrary, GA's ethoxy side group appears to make hydrophobic interactions with Tyr337 which produces a similar downward shift. Without this access, it is much more difficult to reactivate. Naturally, Tyr337 within GB-inhibited hAChE is not allowed to shift downward. The "Y" shaped side group lacks any potential hydrophobic interactions with Tyr337 and, at the same time, the side group is not large enough to cause any steric blocking of Tyr337. This opens up the active site, allowing HI-6 to travel further towards the nerve agent and Ser203 which appears to allow for reactivation of the inhibited hAChE. Additionally, both Y341 and Y124 are making accommodations based on where HI-6 is in order to stabilize with potential pi stacking and t-shaped stacking. Once the structural analysis was complete, additional Ellman's assays were performed to gain

knowledge on each nerve agents reactivation kinetics. As expected, GA-inhibited hAChE demonstrated a very low maximum percent reactivation while GB-inhibited hAChE had a very high maximum percent reactivation. Additionally, soman-inhibited hAChE had a moderate maximum percent reactivation which further supports our structural data.

Futural impact

Throughout this research, the molecular underpinnings of G-series nerve agents were uncovered. Previously, multiple G-series agents were adequately reactivated via HI-6 intervention, however tabun proved to be highly resistance to this reactivator. With high resolution crystal structures and enzymatic data available now, understanding tabun's defiance is much clearer. This now allows for a more accurate optimization of current reactivators to accommodate for the shifts in Phe-295 and Tyr337 or for the creation of entirely new reactivators able to combat tabun's unique intermolecular interactions within hAChE.

There are a multitude of changes that could potentially aid in the creation of a more generalized and efficacious reactivator. An obvious, but possibly effective, change would be to lengthen the middle linker region between the two rings. Due to the steric hindrance caused by Tyr337 in the active site of GA-inhibited hAChE, HI-6 appears to be essentially blocked from entering further. Increasing the length of the linker region would possibly allow for a conformational change of the reactivator in order to bend its way into the active site and hydrolyze the inhibitor presence.

Another proposed optimization of reactivators would be to lengthen the oxime arm instead. This change follows along the same idea as the previous, which is to bring the reactivator closer to Ser203 and the inhibitor. With a longer oxime arm, the entire

reactivator itself would not be forced to move deeper into the active site, instead the oxime arm would be able to reach the inhibitor from the comfortable environment it already inhabits.

There are numerous other modifications that could potentially create a more efficacious therapeutic that could reactivate human acetylcholinesterase no matter what inhibitor is present. That is the end goal. When a soldier is exposed to an unknown chemical agent, there is no time to question which nerve agent it could be. Soldiers use their auto-injector and hope that whatever reactivator the government is providing, will successfully reactivate hAChE. The invention of a reactivator that is able to effectively reactivate hAChE inhibited by tabun, VX, soman, sarin, or any other nerve agent present is what a soldier needs and deserves. The protection of military personnel and the public are of upmost importance and are one of our duties as researchers and scientists.

APPENDIX A

SUPPLEMENTAL INFORMATION FOR CHAPTER 2

Figure S1.1 Crystal structures of Human Acetylcholinesterase in complex with G-series nerve agent. (a) Wall-eyed stereoview of GA (salmon) bound to the active site of hAChE (pale cyan) with hAChE $F_o - F_c$ density scaled to 3σ (green mesh). (b) Wall-eyed stereoview of GB (dark violet) bound to the active site of hAChE (blue-grey) with hAChE $F_o - F_c$ density scaled to 3σ (green mesh). (c) Wall-eyed stereoview of GD (silver) bound to the active site of hAChE (wheat) with hAChE $F_o - F_c$ density scaled to 3σ (green mesh). (d) Wall-eyed stereoview of GF (dark red) bound to the active site of hAChE (light yellow) with hAChE $F_o - F_c$ density scaled to 3σ (green mesh). (e) Wall-eyed stereoview of GP (dark grey) bound to the active site of hAChE (light orange) with hAChE $F_o - F_c$ density scaled to 3σ (green mesh).

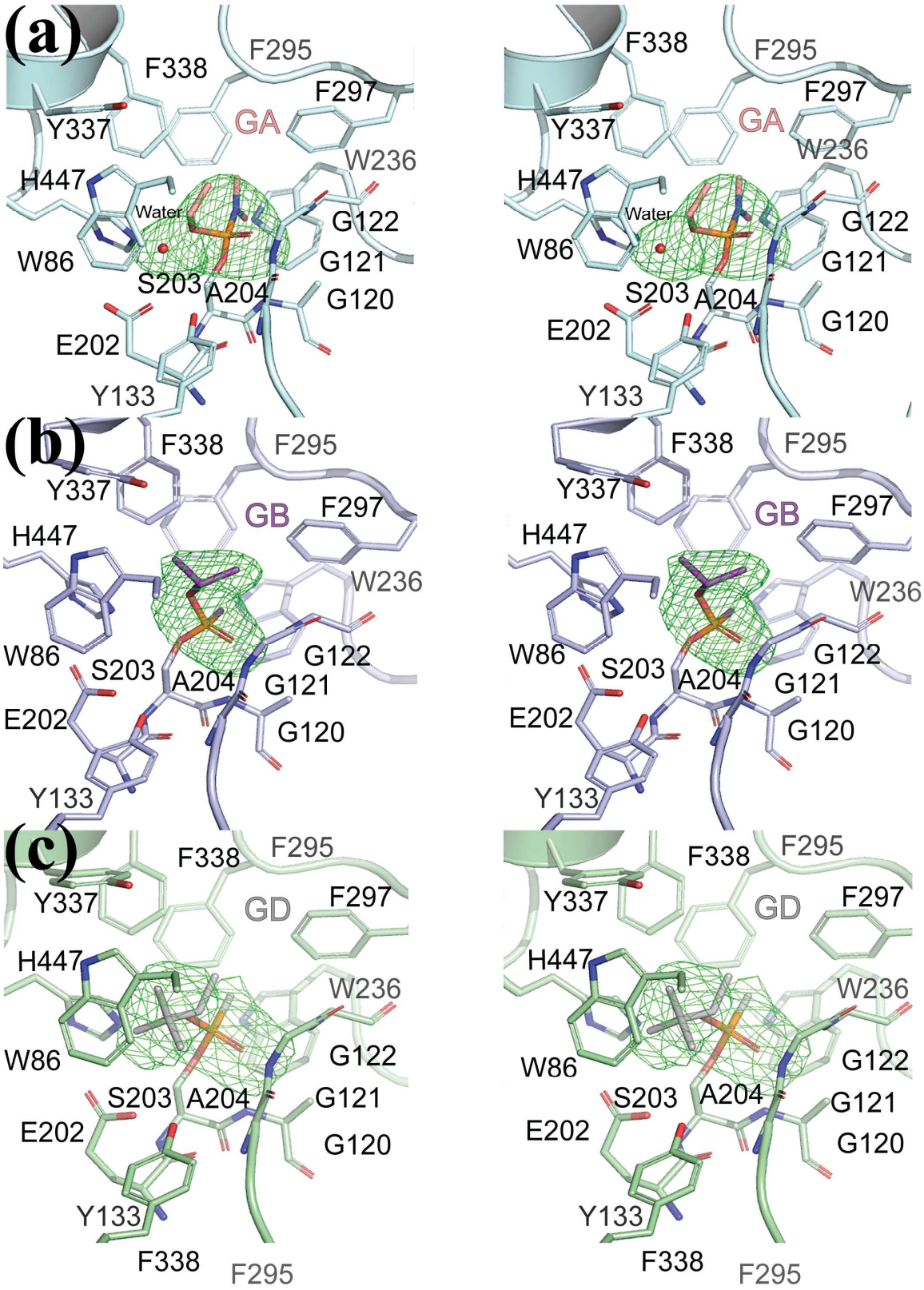
(a)
F338
F295
F297
Y337
GA
W236
H447
Water
G122
W86
G121
S203
A204
G120
E202
Y133
F338
F295
F297
Y337
GA
W236
H447
Water
G122
W86
G121
S203
A204
G120
E202
Y133
(b)
F338
F295
Y337
GB
F297
H447
W236
W86
S203
A204
G122
G121
E202
G120
Y133
F338
F295
Y337
GB
F297
H447
W236
W86
S203
A204
G122
G121
E202
G120
Y133
(c)
F338
F295
Y337
GD
F297
H447
W236
W86
G122
S203
A204
G121
E202
G120
Y133
F338
F295
F338
F295
Y337
GD
F297
H447
W236
W86
G122
S203
A204
G121
E202
G120
Y133
F338
F295

Figure S1.1 Continued

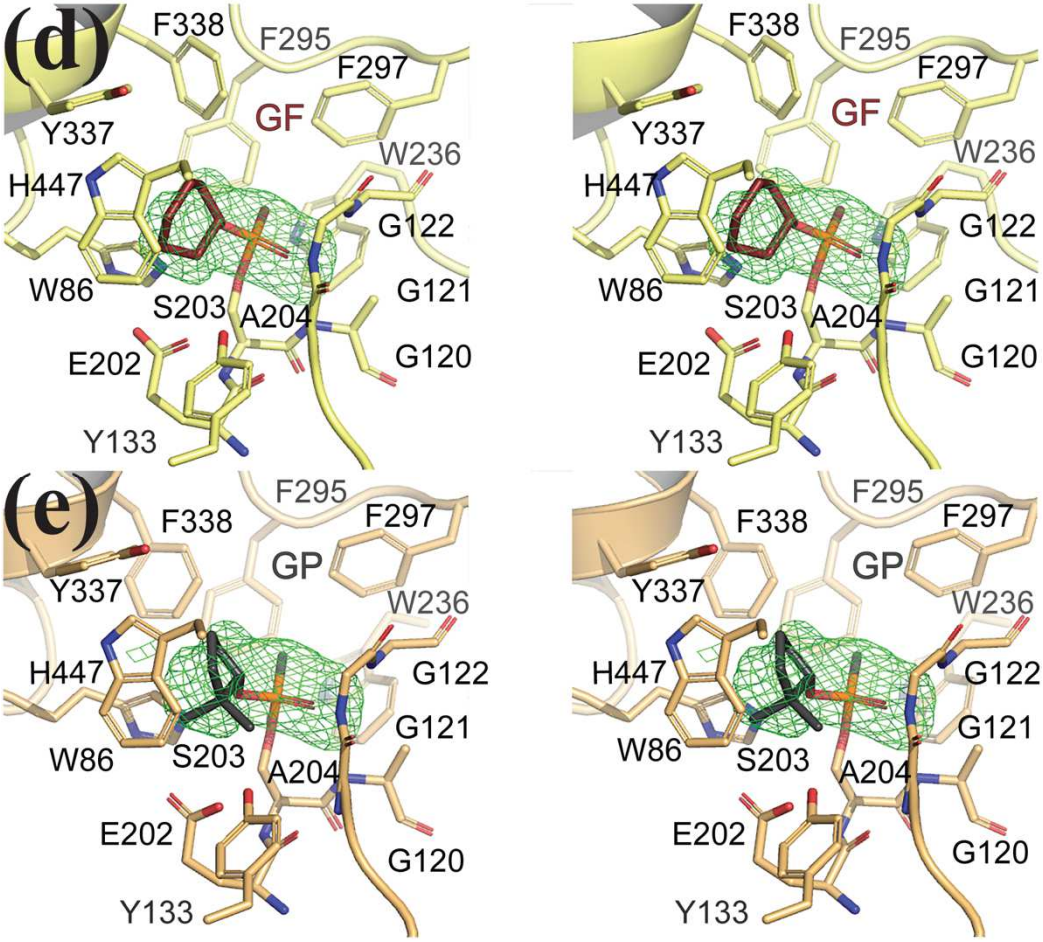

Figure S1.2. Crystal structures of HI-6 bound in the active site of hAChE. (a-b) Wall-eyed stereoview of the active site of hAChE (grey-green) bound to two conformations of HI-6 (orange and pale yellow). $F_o - F_c$ density scaled to 3σ (green mesh). (c-d) Wall-eyed stereoview of the active site of hAChE (light pink) bound to two conformations of HI-6 (light teal and dark teal). $F_o - F_c$ density scaled to 3σ (green mesh). (e) Wall-eyed stereoview of the active site of hAChE (wheat) bound to HI-6 (dark red). $F_o - F_c$ density scaled to 3σ (green mesh). Waters are shown as red spheres.

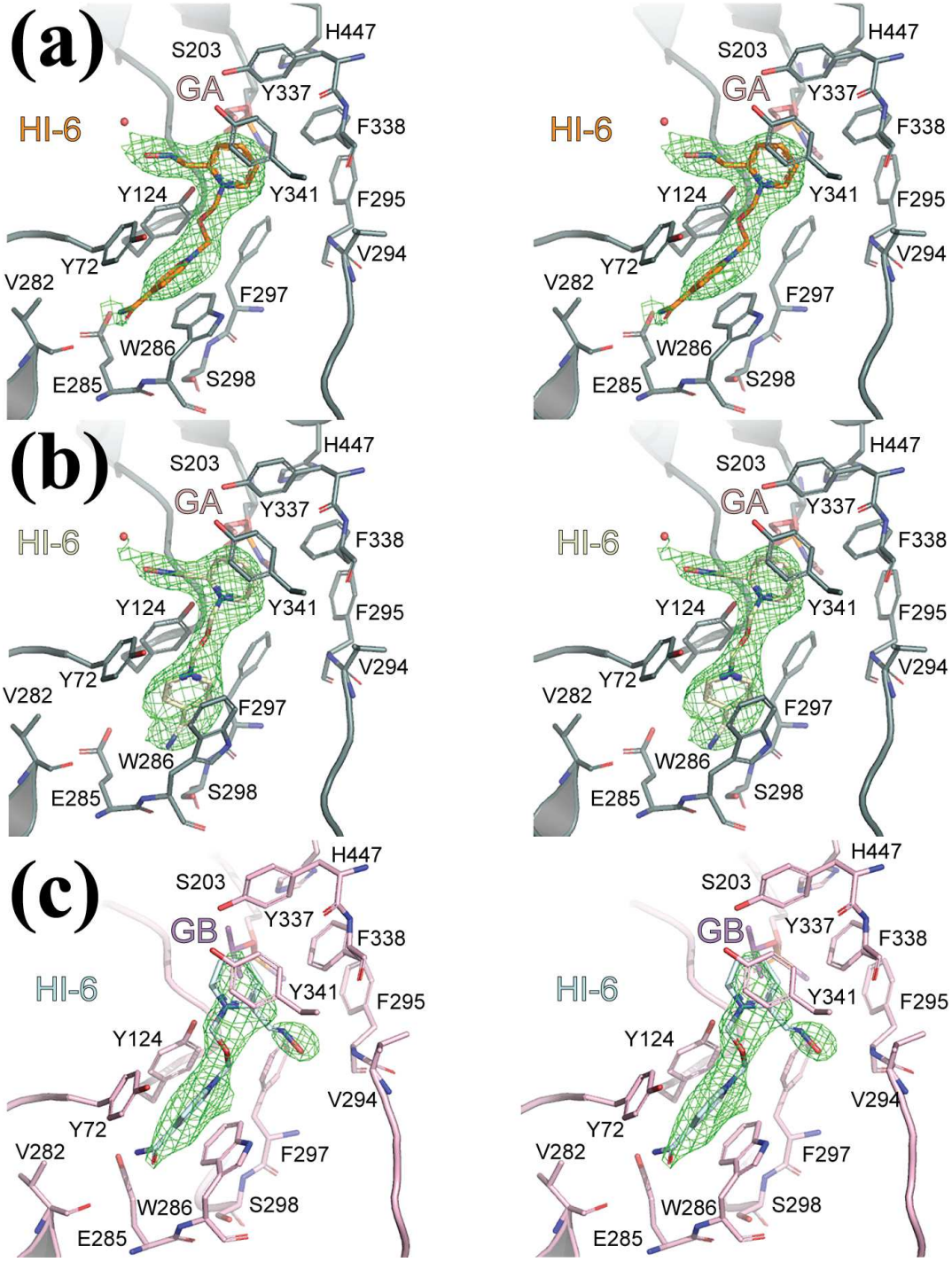
(a)
S203
H447
GA
Y337
HI-6
F338
Y124
Y341
F295
V294
Y72
V282
F297
W286
E285
S298
(b)
S203
H447
GA
Y337
HI-6
F338
Y124
Y341
F295
V294
Y72
V282
F297
W286
E285
S298
(c)
S203
H447
GB
Y337
F338
HI-6
Y341
F295
Y124
V294
Y72
V282
F297
W286
S298
E285

Figure S1.2 Continued.

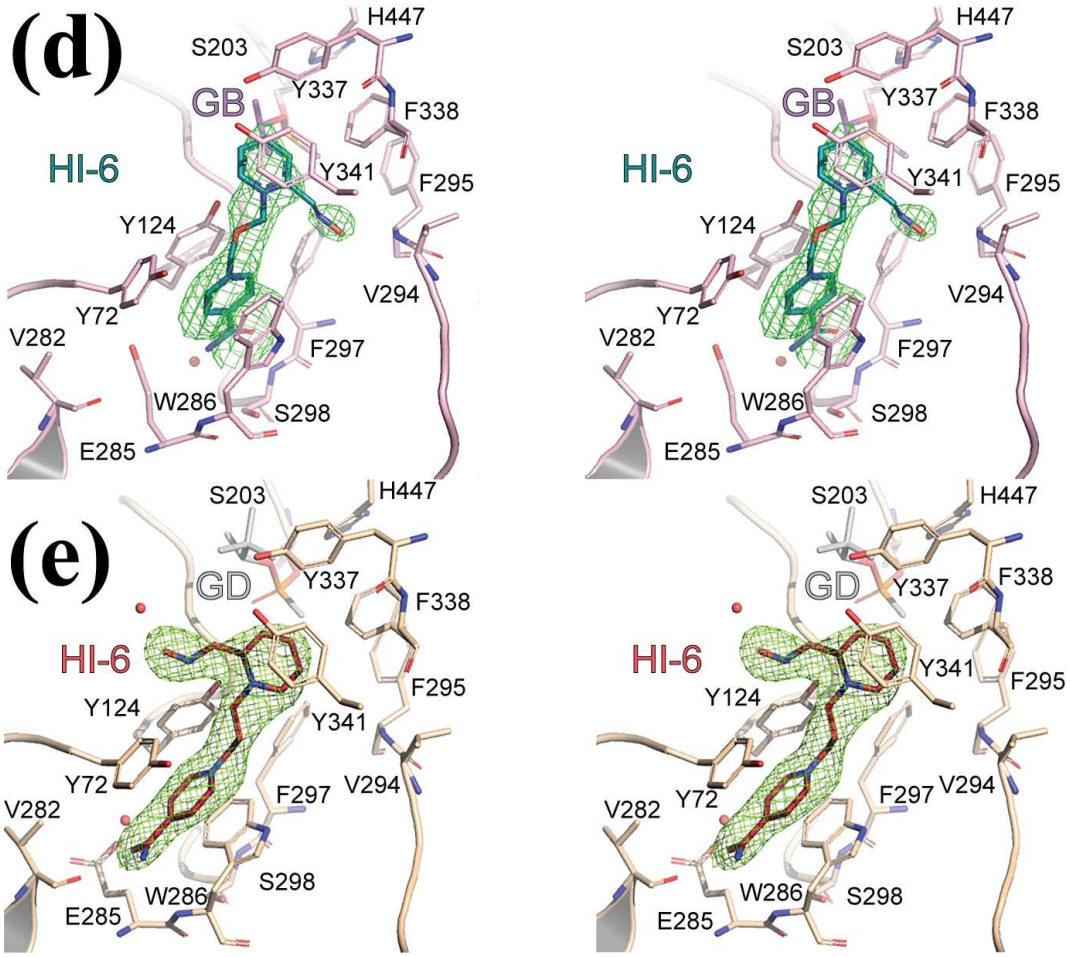

Figure S2.1 Percentage activity of GB with HI-6

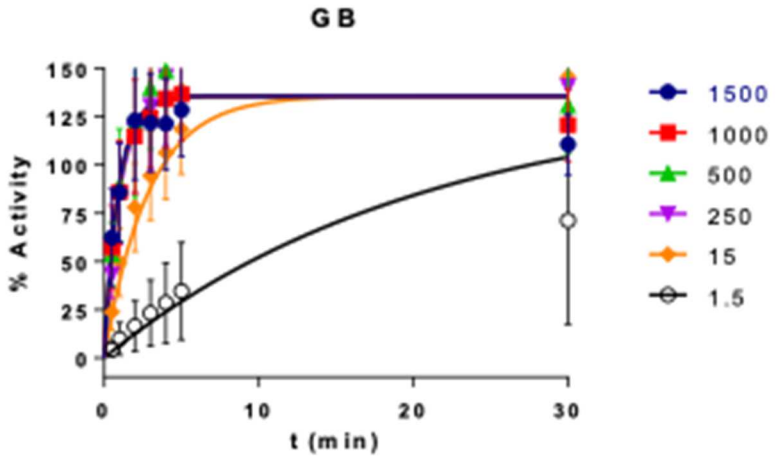

Figure S2.2 Percentage activity of GP with HI-6